1-1-2017

Turbulent Spray Combustion Modeling Using Direct Integration Of Chemistry And Flamelet Generated Manifolds

Ashraya Goyal
Wayne State University,

TURBULENT SPRAY COMBUSTION MODELING USING DIRECT INTEGRATION OF CHEMISTRY AND FLAMELET GENERATED MANIFOLDS

by

ASHRAYA GOYAL

THESIS

Submitted to the Graduate School of Wayne State University,

Detroit, Michigan

in partial fulfillment of the requirements for the degree of

MASTER OF SCIENCE

2017

MAJOR: MECHANICAL ENGINEERING

Approved by:

_____

Advisor: Date:

DEDICATION

I dedicate this thesis to my parents, Yavanika Goyal and Atul Goyal, and brother Abhas Goyal for their endless love, support, and encouragement to work hard for the things that I aspire to achieve.

ACKNOWLEDGEMENT

I would like to express my special appreciation and thanks to my advisor Professor Dr. Omid Samimi for giving me the opportunity to work in his Combustion Physics Laboratory and as Graduate Teaching Assistant for the Intermediate Fluid Mechanics course. His constant support, patience and encouragement have always motivated me throughout my master thesis. Dr. Samimi has encouraged me to experience, learn, and strengthen my knowledge throughout my graduate studies at Wayne State University. With his guidance, I have expanded the theoretical knowledge about my research, as well as applied it practical issues beyond the textbooks. I greatly appreciate the time and effort he spent with me analyzing the data and sharing his profound knowledge during the writing of my thesis. My sincere thanks to, Dr. Henin and Dr. Leela Arava, for being my thesis committee members and providing me their support. I am obliged to Dr. Henein for sharing his knowledge regarding internal combustion engines. I also thank my lab mates for their support. It was a great learning experience for me to work with them in the Combustion Physics Laboratory (CPL). I am also grateful to my friends especially Swapnil Sharma for his support and guidance for their support and motivation throughout my master's degree. Finally, I want to thank my family for their relentless support and encouragement during every step towards completion of my studies and helping me to be where I am today.

TABLE OF CONTENTS

LIST OF TABLES

LIST OF FIGURES

ABBREVIATIONS

AMR	Adaptive Mesh Refinement
ARL	Army Research Laboratory
ASI	After Start of Injection
CFD	Computational Fluid Dynamics
CFL	Courant–Friedrichs–Lewy
CPF	Constant-Pressure Flow
CSP	Computational Singular Perturbation
CT	Computed Tomography
CVP	Constant-Volume Preburn
DNS	Direct Numerical Simulations
ECN	Engine Combustion Network
EGR	Exhaust Gas Recirculation
FGM	Flamelet Generated Manifold
HRJ	Hydrotreated Renewable Jet
IPK	Iso-Paraffinic Kerosene
JP	Jet Propellant
KH	Kelvin-Helmholtz
LES	Large Eddy Simulation

LOL	Lift-Off-Length
MPI	Message Passing Interface
NTC	No Time Counter
PFR	Plug Flow Reactor
PISO	Pressure Implicit with Splitting of Operators
PSR	Partially Stirred Reactor
RANS	Reynolds-Averaged-Navier-Stokes
RNG	Re-Normalized Group
RT	Rayleigh-Taylor
SLF	Steady Laminar Flamelet
SOC	Start Of Combustion
SOI	Start Of Injection
TCI	Turbulence Chemistry Interactions

CHAPTER 1

1 INTRODUCTION

1.1 Chapter Overview

The following chapter is an extensive literature review covering the following topics: types of combustion models used in modern diesel engine research, the importance of Computational Fluid Dynamics (CFD) modeling to reduce fuel emissions, types of turbulence models used in the simulation, mesh sensitivity analysis, sprays basics, and techniques used to determine various parameters in diesel engine turbulent spray combustion, such as pressure based ignition delay, lift off lengths, vapor, and liquid penetrations etc.

1.2 Literature Review

To understand the physics and chemistry behind combustion, two basic models are used in modern combustion research: thermodynamics based and fluid dynamics based models. In the thermodynamic based model, analysis is done using equations based on energy conservation, while in the fluid dynamic based model analysis is done using fluid motion. Fluid dynamics based multidimensional modeling is widely used as it provides detailed geometric information on the flow field based on the solution of the governing flow equations and can provide detailed knowledge about combustion [1]. This model includes turbulent spray combustion modelling. Studies in understanding the physics and chemistry behind the combustion fluid are increasing because of the importance of pollution control and process optimization. In this regards CFD plays a vital role in the

modern combustion industry. Due to increasing speeds of modern supercomputers, Computational Fluid Dynamics (CFD) modeling has been widely applied to support and predict combustion data. Computational fluid dynamics is widely used in engine and turbine design to deepen our knowledge of fuel combustion processes, reduce engine development costs and enhance the design with accurate reaction mechanism. Prior research has shown the superiority of this process, which also forms the backbone of the simulation and modeling [2].

Turbulent spray combustion is a complex and compounded process involving sprays, turbulence, autoignition, droplets interactions and multi-phase flows. Due to its multi physics nature, this process is the backbone of the turbine and diesel engine combustions, which has made it an important area of research for many years. Understanding the physics of the spray formation is one of the major ongoing research area in both experimentation, and modeling. The main concentration of the spray experimentation is to quantify the lift-off length (LOL), spray penetration, vapor penetration and species mass fractions. A variety of data can be found in [3]. The simulation attempts to model what we gather in the combustion chamber with minimum theoretical error, and then proceed forward to predict what we cannot measure or quantify in experimentation due to high pressure and temperature of the combustion environment, or unavailability of instrumentation. Due to the very complex nature of the spray, simulation is widely accounted for simplifying and modeling (versus solving) of the spray physics. As an example, there is still no solution (or well-validated model) for droplets interaction and break up kinetics of heavy hydrocarbons, and turbulence model with comprehensive coefficients (e.g. RNG RANS versus Standard RANS). In this regard, some

of the simulation works are turbulence modeling [4], mesh size effect [5] and droplet breakup models [6]. In the multidimensional numerical simulations, spray behavior is a fundamental part of diesel engine combustion research for understanding the in-cylinder combustion phenomenon. Spray behavior is described as a multiscale and turbulent spray process. Aerodynamic interactions between the molecules affects the liquid core region which makes the liquid surface unstable. Liquid ligaments are created due to instability which in turn creates the parent droplet, also called primary break, which is followed by creation of child droplets known as secondary breakup. Size of the droplets are reduced due to evaporation and combustion occurs while reduced droplets are travelling downstream from the injector nozzle.

To reach efficient combustion and minimization of emissions, optimization of turbulent spray combustion is needed both experimentally and computationally. There are many studies regarding turbulent spray combustion modeling, e.g., [7-8] and experimental studies, e.g., [9-10]. The Engine Combustion Network (ECN) [11] of Sandia National Laboratories provides experimental data for turbulent spray combustion using several types of fuels and fuel surrogates such as diesel#2, biodiesel, IPK (Iso-Paraffinic Kerosene), HRJ (Hydrotreated Renewable Jet), JP-8 and n-dodecane. The measurements at Sandia National Laboratories are conducted using two types of combustion chambers: Constant Volume Chamber, also called Constant-Volume Preburn (CVP), and Constant-Pressure Flow (CPF) in which high temperature and pressure conditions are controlled. The experiments are performed using different types of injectors such as Spray A to D, which differ in operating and boundary conditions, orifice diameters, spray angles and number of holes. Spray A is used in this thesis for modelling purpose which uses a single component diesel surrogate

fuel (n-dodecane), a single hole injector (common rail, 1500-bar fuel pressure, 363-K fuel temperature), representing a diesel engine combustion condition (900 K, 60 bar) that uses a moderate rate of exhaust-gas recirculation (EGR). There have been studies to analyze how Spray A behaves in different combustion vessels. Using a constant volume chamber, Siebers et al. [12] described the spray liquid penetration length at near Spray A conditions and studied the spray behavior when operating conditions such as decreasing injector orifice diameter, injection pressure, ambient gas density or temperature, and changing fuel volatility. It was found that liquid length is independent of injection pressure, increases with fuel volatility or temperature and decreases linearly with injector diameter, temperature, or density. Weber et al. [13] used a constant pressure flow chamber at diesel conditions of 50 bar and 800 K, to provide optimization strategies for spray penetration and mixture formation both experimentally and computationally. Kweon [14] at ARL using surrogate fuel, JP-8 and optical diagnostics (Schileren Images and Mie Scattering) analyzed the effects of injector configuration and fuel composition by varying cetane number in constant pressure chamber. Payri et al. [15] studied the fuel-temperature effect in non-reacting and reacting diesel sprays using a novel injector and imaging diagnostics for liquid phase penetration, light-off length, and ignition delay measurements and reported that lesser degree to reacting and nonreactive sprays depend on the injector body temperature and real fuel temperature. New advanced x-ray techniques and medical imaging have been used for resolving the structure of the spray's liquid core. Wang et al. [16] used x-ray phase contrast imaging to study the near nozzle atomization process of air assisted water sprays and observed atomization processes at high-We numbers, such as jet narrowing, spray breakup, and the tracking of the mass volume fraction. Coletti et al. [17]

used x-ray computed tomography (CT) technique to provide detailed information of the spray dense region. These studies have provided new insights into the spray including the near nozzle region, improving our understanding, and driving the generation of enhanced spray models which widens the area of research in the simulation community.

Computational Fluid Dynamics (CFD) modeling has been widely applied to support and predict combustion data. Over the years many CFD solvers have been developed for designing and research purposes in the CFD based engine research. Some of them are CONVERGE developed by Convergent Science, USA [18]; KIVA, developed by Los Alamos National Laboratories [19]; OpenFoam developed by OpenCFD [20]; and AVBP developed by Centre Européen de Recherche et de Formation Avancée en Calcul Scientifique (CERFACS). These multidimensional solvers utilize experimental data and carry out model-validation studies and quantify the simulation error. According to the report by Luis Bravo et al. [21] a validation study reveals the suitability of modeling assumptions (physical models), stability of the spatio-temporal numerical technique (numerical methods), and calibration of model parameters (turbulence, breakup, combustion constants) that are required to optimize the simulation.

The ultimate goal of turbulent spray combustion modelling is prediction of ignition delay based on pressure rise and/or luminosity using pressure, temperature, species histories and fuel vapor penetration [22]. Various turbulent modeling such as Direct Numerical Simulations (DNS) [23], Reynolds Averaged Navier-Stokes (RANS) [24], Large-Eddy Simulation (LES) [25] and its types such as Smagorinsky–Lilly based LES model and RANS based k-ε model [26] have been used to compare and find the best approach to turbulent spray combustion modeling. DNS can completely resolve all the

relevant flow scales. However, the computational cost associated is not feasible for engine studies. (RANS) which is based on averaged governing equations is unable to predict the local unsteadiness in the flow. An LES approach, based on spatially filtered governing equations, can capture the large-scale flow structures based on the filter size. A flaw with this approach is that the unresolved small-scale structures are still modeled. Since LES can capture local unsteadiness and is computationally more feasible than both DNS and RANS, LES is widely utilized for simulation of internal combustion engines and turbines [26]. However, LES results are mesh dependent, in other words, different outcomes may be realized by decreasing mesh size [27].

Reducing the number of intermediate species and solving combustion kinetics plays important roles in turbulent spray combustion modeling. There are many detailed chemistry solvers. One of the most widely used solvers is SAGE, [28] which uses local conditions to calculate reaction rates based on the principles of chemical kinetics. The solver is fully coupled to the flow solver, and the chemistry and flow solvers parallelize independently of one another. This solver has been widely used in combustion applications such as pre-mixed, partially premixed and non-premixed burns, along with auto ignition of multiple fuels. The SAGE solver could be computationally very expensive depending on mechanism size, since it calculates reaction rates for each elementary reaction along with transport equations.

Van Oijen and Goey [29] formulated a method called FGM (Flamelet Generated Manifolds) by generalizing the Steady Laminar Flamelet method (SLF) to speed up the calculation. It assumes that the multi-dimensional flame can be considered a sum of one-dimensional flames, making thermochemical states in the turbulent flame, similar to those

in 1-D laminar flame modeling. In FGM, two scalars represent chemical mechanisms and composition: mixture fraction and progress variable. A look-up table with a particular type of flamelet retrieves thermochemical information as a function of variables: mixture fraction, temperature, pressure, scalar dissipation rate and combustion progress variable before simulation, which reduces the runtime.

There are three types of flamelets, depending upon requirements: 0-D ignition, 1-D diffusion, and 1-D premixed [30]. The look-up table for 0-D ignition flamelet has a manifold dimension with four variables: mixture fraction, progress variable, temperature, and pressure. 0-D is usually utilized for homogenous reactors such as partially stirred reactor (PSR) and plug flow reactor (PFR). 1-D diffusion flamelets are used for stationary turbulent non-premixed flames such as coal-fired turbines and liquid fuel gas turbines. The generated manifolds in the lower and upper branches are modeled with extinguishing flamelet. 1-D premixed flamelets are often used for turbulent premixed flames such as land-based turbines. The generated manifold is modeled with adiabatic freely propagating flame. Both 1-D diffusion and premixed flamelets assume that heat loss does not affect the species composition. For these two flamelets, the manifold dimension is two, with the calculated look up table containing progress variable, mixture fraction, enthalpy, and variance of mixture fraction.

1.3 Organization of Thesis

In this thesis, tabulated chemistry with various mesh refinements is utilized to reduce the computational time and refine local grid based on temperature and velocity gradients. The main objective of the current research activity is to study and find the effect

of mesh size on pressure rise due to combustion using various mesh refinement levels and compare the performance of two kinetics solvers, SAGE and FGM, at engine relevant conditions using different turbulence models. This thesis is organized by briefly by first presenting computational methodologies and CFD sub models followed by results and discussions.

CHAPTER 2

2 NUMERICAL METHODOLOGY

2.1 Chapter Overview

The following chapter discusses the computational parameters used for running the simulations, followed by sprays and their primary and secondary break ups. The importance of modelling turbulence in combustion, and different types of turbulence modeling approaches used in the modern simulation world are also reviewed. Types of combustions models used to solve the detailed chemistry and the pressure triangulation correlation to correct pressure rise timing is also explained.

2.2 Computational Methodology

This section will discuss the computational methodology used for running the simulations. This chapter includes the CFD solver used, computational algorithms, operating parameters, and boundary conditions of the constant volume chamber and the Spray A injector, and mesh characteristics using grid scaling, embedding and adaptive mesh refinements.

2.2.1 Computational Algorithm

The CONVERGE CFD package [30] was utilized to solve the governing equations. In this thesis, all the transport equations and momentum were solved using the finite volume method (second order central accurate spatial discretization scheme and first order implicit in time). In other words, in order to maintain stability, time accuracy was set to first order by running fully implicit and both the temporal and spatial domains were

discretized using the implicit second-order central difference schemes. Pressure-velocity coupling was accomplished using the Pressure Implicit with Splitting of Operators (PISO) method of Issa [31]. The liquid/gas coupling was accomplished using a nearest node approach to exchange mass, momentum, and energy terms of a parcel (Lagrangian particle) with the fluid-phase (Eulerian field) values of the closest computational node [32]. A Taylor series expansion was used to calculate the gas velocity (Eulerian field) at the location of the parcel (Lagrangian particle). Operating conditions were temperatures ranging from 900 K to 1200 K, pressure of 7.94 MPa, and density of 22.8 kg/m^3. Variable time-stepping was used i.e. the time-step was automatically calculated for each computational cycle based on the maximum allowed CFL numbers (based on velocity CFL#1, viscosity CFL#2.5, and speed of sound CFL#50), as well as spray, evaporation, and combustion time-step control methods [33].The simulations were performed using parallel computations on distributed memory machines using the Message Passing Interface (MPI).

2.2.2 Sandia Constant Volume Chamber and ECN Spray A

For comparisons of the simulation results, with the experimental data was taken from open data search utility on the ECN website. Constant volume chamber and Spray A were used in this thesis. The experimental set up of the constant volume chamber at Sandia National Laboratories and combustion vessel pressure history by the diesel experimental conditions are shown in Figure 2.1 and Figure 2.2 , respectively. The experimental facility also provides full optical access for line of sight or orthogonal optical diagnostics as seen in Figure 2.1 shows the setup with the positioning of the high-pressure common rail fuel injector, number of spark plugs, and fan location. To prevent wall impingement effects

interfering during spray diagnostic process, the characteristic length of the vessel is typically designed to be 100 mm on each side. To prevent condensation of combustion products on the windows the vessel walls are heated electrically to engine surface temperatures. Multiple spark plugs are used to provide consistent ignition of a preburn lean mixture.

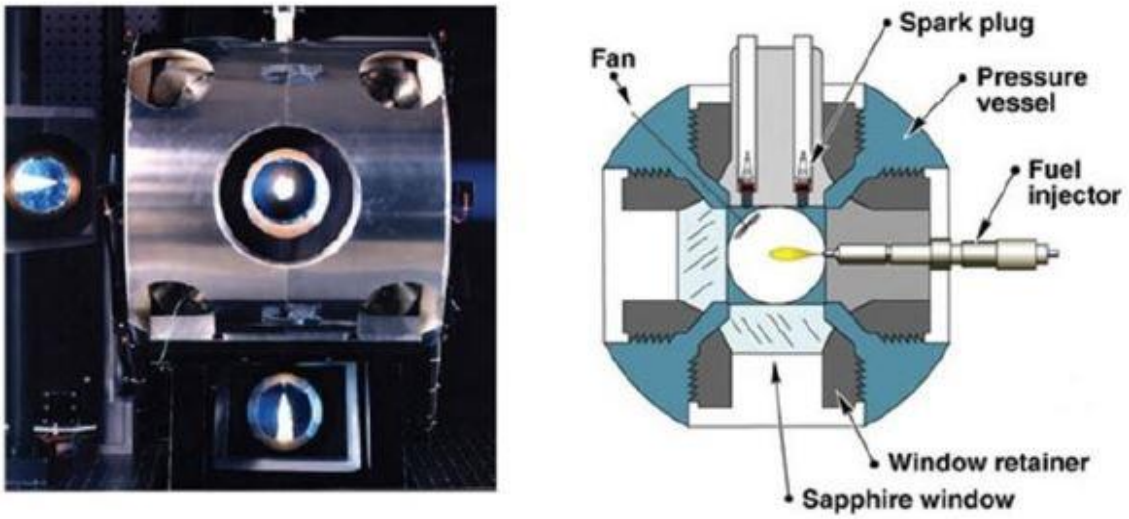

Figure 2.1 Sandia National Laboratories Constant Volume Chamber [11], (a) Optically accessible high-temperature, high-pressure spray chamber (left), (b) Schematic of combustion vessel (right)

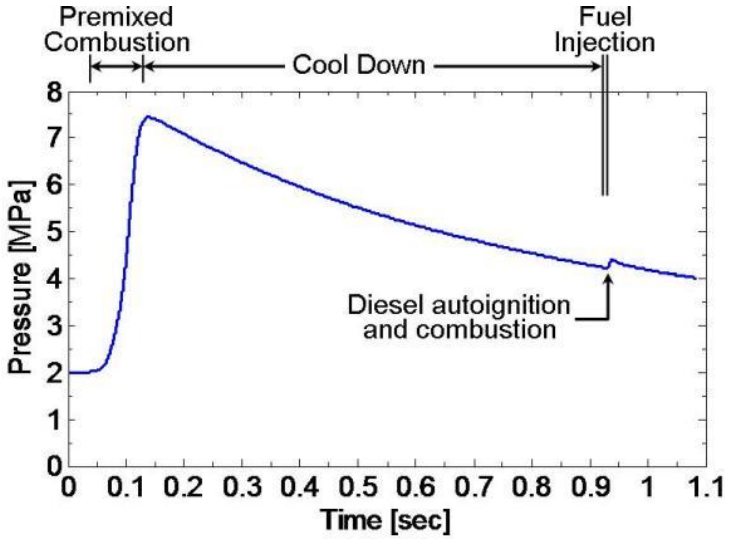

Figure 2.2 Combustion vessel pressure history [11]

At the start of the experiment, to meet the desired pressure and temperature, the vessel is filled to a specified density with a premixed, combustible gas mixture, this mixture is then ignited with spark plugs creating a high-temperature, high-pressure environment through an initial premixed combustion. The combustion products cool over a relatively long period of time (~1 s) due to heat transfer to the vessel walls and interaction with the vessel walls, thus decreasing the pressure of the chamber slowly. The ambient gas temperature, density, and composition at injection are determined by the pressure at the time of fuel injection and the initial mass and composition of gas within the vessel. When the desired experimental conditions are reached, the diesel fuel injector is triggered and starts the spray process and results in auto-ignition and combustion processes as shown by the second pressure rise in Figure 2.2 around 0.9 s.

Spray A conditions are provided in Table 2.1 . The physical description corresponds to an evaporating fuel spray with 0% oxygen content (nonreacting), developing at diesel engine ambient conditions. A single hole, modern common rail injector with an injector

diameter of 90 μ (Bosch CRIN 2.4) is used at typical diesel injection pressures [34]. A single component diesel surrogate fuel (i.e., n-dodecane) is used due to its extensively well-characterized chemical and physical properties. Detailed and reduced mechanisms for n-dodecane are readily available from the literature [35].

Table 2.1 Spray A Injector Specifications

Sandia Conditions	**Value**
Fuel	n-dodecane
Ambient composition	0% Oxygen (Non- reacting)
Ambient temperature (K)	900
Ambient density (kg/m^3)	22.8
Number of injector holes	1 (axial)
Injection Pressure (MPa)	150
Fuel Temperature (K)	363
Nozzle Diameter (mm)	0.09
Injection Duration (ms)	1.5
Injection mass (mg)	3.5

2.2.3 Boundary Conditions

The domain had a cylindrical shape with a diameter size of 108 mm and length of 108 mm, which is the same as the SANDIA National Lab vessel dimension. A cubical shape was also investigated and did not have an effect on timing of pressure-based ignition delay. The wall temperature was set to 461 K for all of the studied cases. The nominal injected pressure, ambient density, and fuel temperature were 150 MPa, 22.8 kg/m3, and 373 K, respectively. The injected pressure was a function of time, shown in Figure 2.3 and the rate shape (flow rate versus time) was implemented in the CFD solver directly. Initial

ambient mixture composition for both cases, non-combusting and combusting evaporating spray, are tabulated below. The initial combustion chamber temperature varies from 900 K to 1200 K.

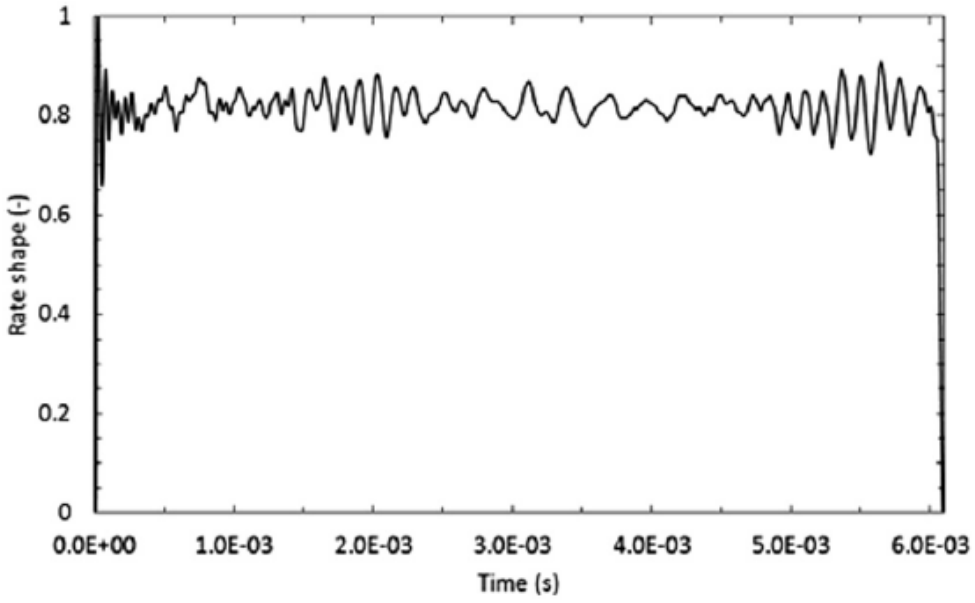

Figure 2.3 Injection rate shape [22]

Table 2.2 Constant Volume Combustion Chamber gas initial conditions and resulting ignition delay times

	Ambient Temperature (K)	**Ambient Composition (Mole fraction %)**	**Experimental pressure-based ignition delay (ms)**
Non-combusting evaporating spray	900	O_2 = 0 N_2 = 89.71 CO_2 = 6.52 H_2O = 3.77	-
Combusting evaporating spray	900 1000 1100 1200	O_2 = 15 N_2 = 75.15 CO_2 = 6.22 H_2O = 3.62	0.41 0.24 0.15 0.11

2.2.4 Mesh Characteristics

The mesh resolution used in this thesis was generated using the modified cut-cell Cartesian grid generation method [36] in CONVERGE where the geometry was immersed into a Cartesian block and the cells at the boundary were trimmed. There are three grid control strategies in CONVERGE: Grid Scaling, fixed embedding and adaptive mesh refinement. Grid scaling reduces the simulation runtime by changing the base grid at specified times and makes the mesh coarse at non critical regions, while refining the critical areas, capturing more insights. If the grid scale is set to zero the mesh size remains unchanged during simulations. If the grid scale is set to a positive value the mesh gets refined. A negative value will coarsen it. Grid scaling was not used in this thesis.

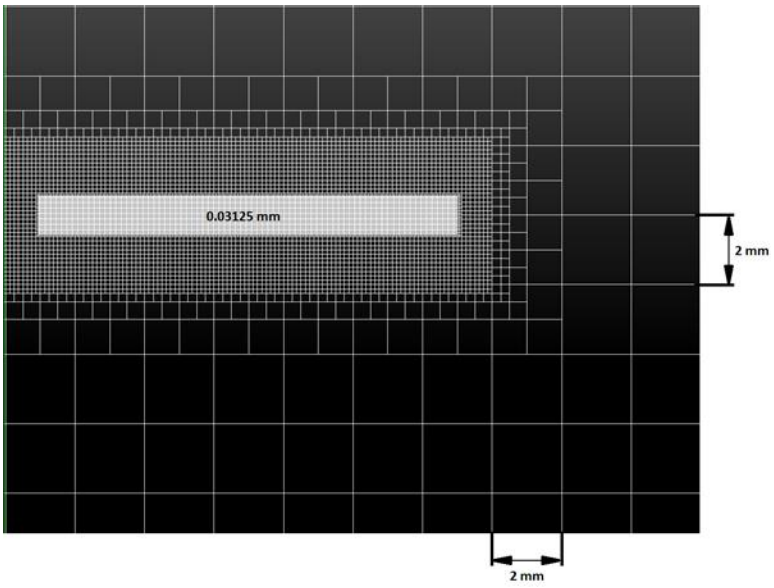

Figure 2.4 Mesh Shape

In this thesis, the mesh was refined at the run-time using two other grid refinement methods available in the software. A coarse mesh was utilized to minimize the solution time. Mesh embedding and adaptive mesh refinement were utilized to fulfill the sub-

models' mesh size requirements (i.e., breakup and collision sub-models). The minimum mesh size of 0.03125 mm was used in modeling. To achieve the mesh resolution of 0.03125 mm, a coarse mesh of 2 mm was used over the whole domain, and the mesh was refined in certain areas to reach 0.03125 mm as shown in Figure 2.4. The first method used is called fixed embedding, in which the grid can be refined in a particular region for a given period of time. The unsteady gas jet model is not incorporated in CONVERGE, and hence fixed embedding is used as a substitute to accurately predict liquid-gas relative velocity by refining the grid around the nozzle during fuel injection. Apart from the region around the nozzle, fixed embedding was implemented on all other boundaries. There are various methods for fixed embedding such as boundary, sphere, cylinder, nozzle and injector, box, and region. Cylindrical mesh embedding with diameter of 1 mm and length of 12 mm was utilized in front of the injector tip to resolve the complex flow behavior at the nozzle exit. The mesh size in the embedding area is fixed and equal to the minimum mesh size of 0.03125 mm.

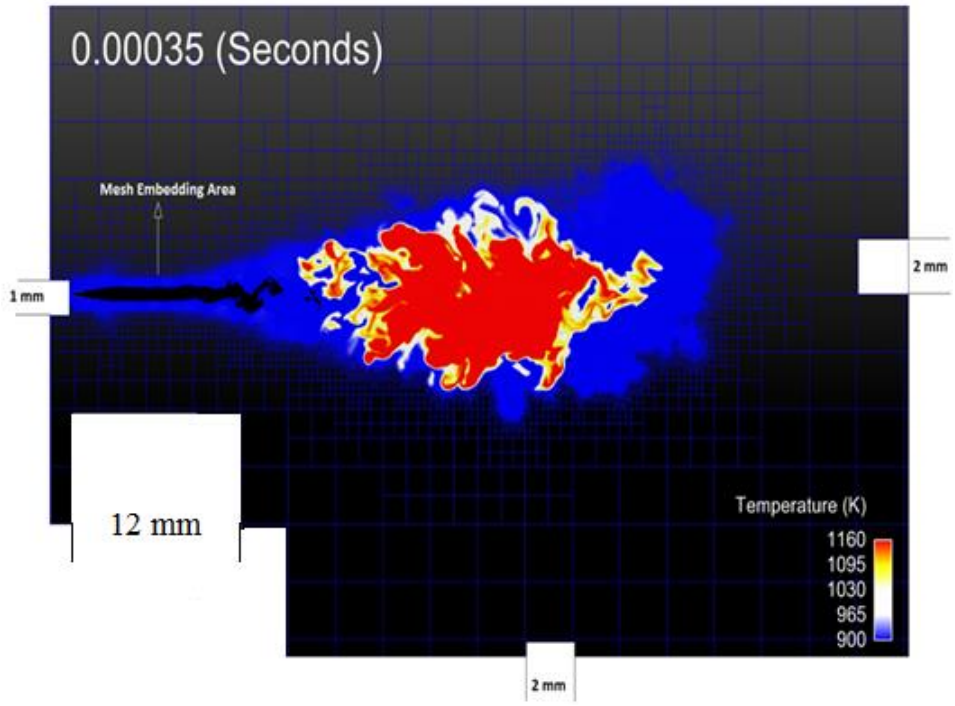

Figure 2.5 Mesh characteristics and temperature profile at 0.00035 s and initial combustion chamber gas temperature of 900 K. The mesh size in cylindrical embedding area (with diameter of 1 mm and length of 12 mm) is fixed and equal to 0.03125 mm

The second grid refinement method, called Adaptive Mesh Refinement (AMR), was also used in the whole domain except in the embedded mesh area as shown in Figure 2.5 . During the run-time, AMR automatically refines the size of the grid cells based on the change in the values of certain fluctuating flow variables and moving conditions, such as temperature and velocity, up to the predefined mesh resolution of 0.03125 mm in this thesis. The flow variables considered in this thesis were temperature and velocity. The limits of these variables were defined as 2.5 K and 1 m/s respectively and were used as sub-grid criteria for activation of AMR.

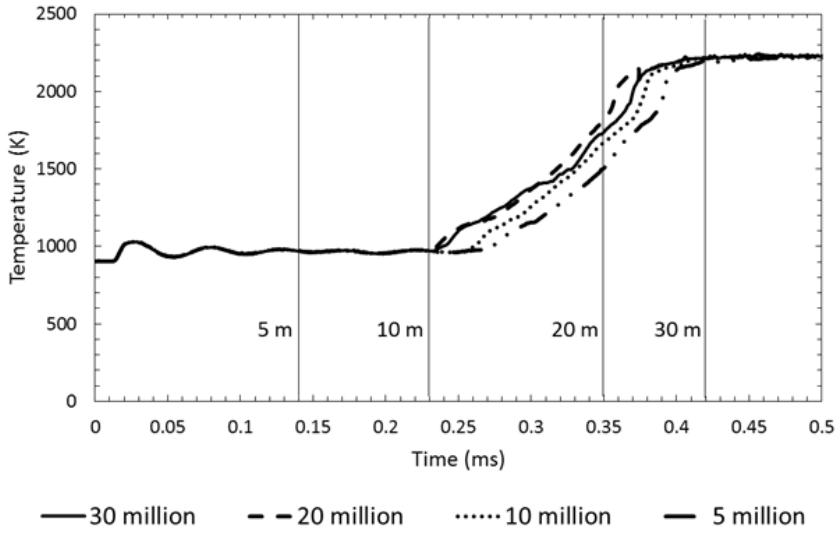

Figure 2.6 Gas temperature rise in combustion chamber using various thresholds for maximum number of meshes. The initial temperature of combustion chamber is 900 K. FGM combustion model and LES turbulence model were utilized

The mesh size was decreased down to 31.25 micron and the total number of meshes was limited to 30 million. The effect of generated mesh numbers on maximum temperature rise at 900 K is shown in Figure 2.6. The above two methods helped in refining the grid in critical regions (spray area) when necessary while keeping the grid in the rest of the region comparatively coarser, thereby saving computation time. The effects of various mesh number thresholds on temperature rise at initial gas temperature of 900 K are shown in Figure 2.6. The temperature rise using 20 million meshes and 30 million meshes are identical. Also, spray simulation duration at initial gas temperature of 900 K is longer than the other cases due to longer ignition delay time. Thus, thresholds of 30 million meshes is utilized for all the cases in current work.

2.3 Spray Sub-Models

The following section will discuss the sprays, the primary and secondary break up of liquid fuel core, with an overview of spray modelling followed by spray break up sub

models used during simulation. The KH-RT spray sub model equations are explained, as well as the evaporation model and injection methods.

2.3.1 Introduction

Spray and atomization processes are defined as multiphase flow phenomenon having a liquid phase and a gas phase. The liquid phase is in the form of droplets and ligaments, while the gas phase is represented as a continuum. An image of the diesel spray atomization process is shown below. Spray plays a vital role in air-fuel mixture and helps in increasing its surface area for rapid evaporation and combustion. This process affects ignition behavior, heat release rates, pollutant formations rates, fuel consumption and exhaust emissions. The kinetic energy of the spray represents the main source for turbulence production and governs the microscale air-fuel mixing by turbulent diffusion and the flame speed of the premixed flame front [37].

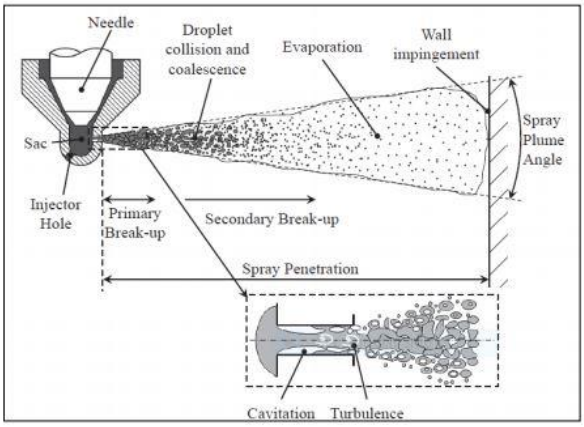

Figure 2.7 Various Stages of high pressure diesel spray breakup [2]

2.3.2 Primary Atomization

The spray process is initiated when high pressure liquid fuel is discharged from an injector nozzle. The liquid fuel stream injected contains important physical properties, such

as liquid-phase turbulent flows, and has cavitation effects from the generation of gas-phase bubbles that implode while travelling downstream of the flow and then are ejected into the combustion chamber. When disruptive forces acting on the liquid surface exceeds the surface tension forces breakup, or disintegration, occurs. Also, external forces such as aerodynamic forces, surface shear forces, centrifugal forces, and electrostatic forces, acting on the liquid surface distorts the bulk liquid and promotes the disruption. These external forces lead to oscillations and perturbations of the interfaces and these oscillations get amplified and results in the breakup of the liquid into smaller droplets. This initial breakup process is called the primary breakup or the primary atomization.

2.3.3 Secondary Atomization

As explained earlier during primary atomization the liquid core region begins to disintegrate into smaller droplets, but still a population of larger droplets produced in the primary atomization are unstable and when they exceed critical droplet size they undergo further disruption into smaller droplets. This process is defined as the secondary breakup or the secondary atomization. In this liquid behavior is defined as the disintegration of larger droplets and ligaments into smaller droplets. The breakup in a single droplet is caused by relative velocities, turbulence, heat and/or mass transfer. Secondary fragmentation of particles occurs due to instabilities caused by the high relative velocities between the deformable liquid droplet and surrounding of fluid.

Therefore, the final droplet size distribution produced in an atomization process is determined by the flow characteristics and the properties of the fluids in both the primary and secondary disintegration. If the surrounding temperature is high enough, the droplets will evaporate producing vapor, which mixes with the oxidizer, forming a combustible

mixture, which ignites due to the presence of sparks, or due to increased pressures and/or temperature in compression-ignition engines. The analysis of atomization and sprays are typically carried out by means of theoretical, numerical, or experimental methodologies [38]. As in traditional fluid mechanics, the characterization of spray behavior is also most conveniently analyzed with several non-dimensionless parameters.

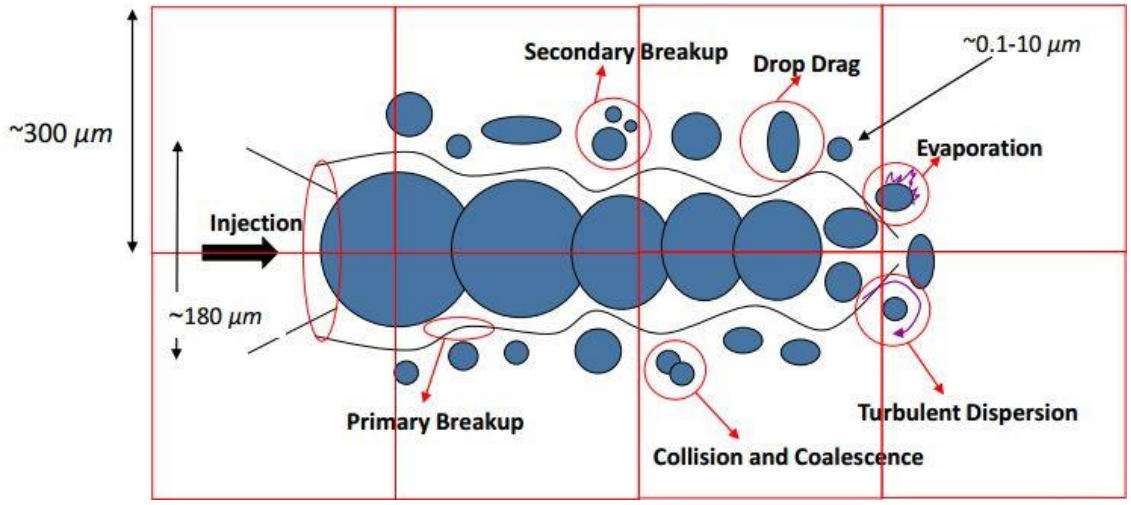

Figure 2.8 Various Stages of high pressure diesel spray breakup [30]

2.3.4 Spray Breakup Models

There are various break up models such as Kelvin-Helmholtz (KH), Rayleigh-Taylor (RT), KH-RT, Modified KH-RT, KH-ACT (Aerodynamics Cavitation Turbulence), Taylor Analogy Breakup (TAB), Linearized Instability Sheet Atomization (LISA) which are used to study breakup in different applications. In diesel spray applications, the instabilities are typically described through KH and RT models, which are used to predict primary and secondary breakup. An intact liquid-core breakup length is used where the KH model alone is used to predict primary breakup; downstream of this critical length (and in the hybrid case) the RT and KH models are implemented in competing manners, such that the droplet breaks up by the model that predicts a shorter breakup time. In the injector

nozzle region, where droplet velocities are larger, the RT breakup model dominates, while in KH model is used further downstream.

The present simulation employed the blob injection method of Reitz and Diwakar 1987, [39] in which parcels of liquid, with characteristic size equal to the effective nozzle diameter, are injected into the computational domain. In diesel engine applications, Reitz [40] and Reitz and Diwaker [41] have used a blob injection model that continuously injects into the gas-phase large drops (blobs) with a diameter comparable to the size of the nozzle hole. The frequency of the addition of new blobs is related to the fuel-injection rate, assuming constant density of the liquid fuel and ideally spherical blobs. The KH model is applied immediately after the injection region to provide the aerodynamic instabilities that will begin to grow on the droplet surface; this causes smaller secondary droplets to be sheared off of the parent droplet surface as depicted in figure below.

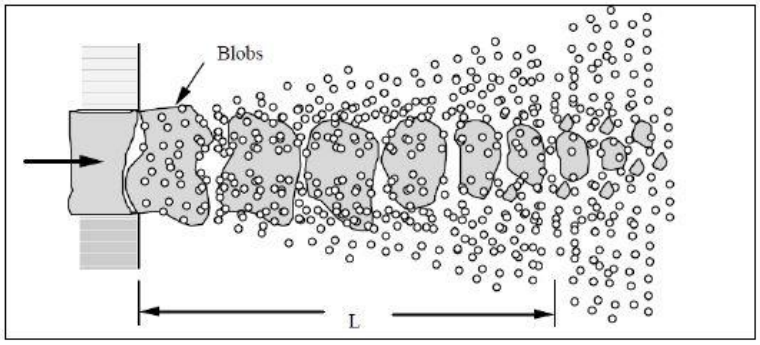

Figure 2.9 Illustration of the blob-injection model of Reitz et al. [40]

The atomization of the liquid blobs and the subsequent droplets were simulated with models based on the Kelvin-Helmholtz (KH) and Rayleigh-Taylor (RT) instability mechanisms. The model coefficients constants are tabulated below.

Table 2.3 Droplet breakup model coefficients

Model	KH-RT model coefficients
KH model coefficients name	**Coefficients' values**
Fraction of the injected mass/parcel to create new droplet	0.05
Shed mass constant	0.10
Model size constant	0.60
Model velocity constant	0.188
Model breakup time constant	4.0
RT model coefficients name	**Coefficients' values**
Model breakup time constant	1.0
Model size constant	0.1
Model breakup length constant	10

Kelvin-Helmholtz (KH) model: This model uses a liquid stability analysis to model the atomization process of relatively large injected parcels. Converge calculates the breakup of parcels and resulting drops by assuming that the breakup drop radius is proportional to the wavelength of the fastest growing unstable surface wave. The formulation of the KH Wave Breakup Model developed primarily by Reitz and Diwaker [40] considers a cylindrical liquid jet of radius a penetrating through a circular orifice into a quiescent incompressible gas chamber. The interaction between the surrounding gas and the liquid jet creates a number of infinitesimal surface perturbations that are characterized with initial amplitude of η_0 and a spectrum of wavelengths λ :

$$k = \frac{2\pi}{\lambda} \tag{2.1}$$

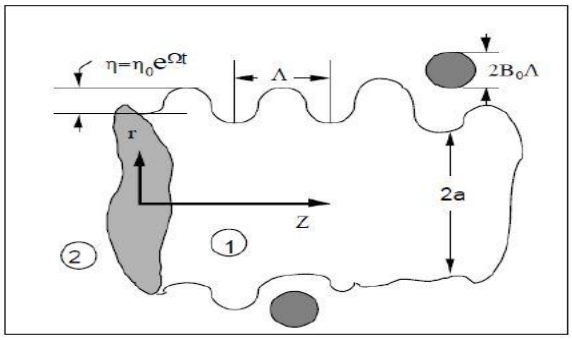

Figure 2.10 Schematic growth of surface perturbations in KH model [41]. Notation 1 depicts the liquid phase, while 2 depicts the gas phase

Rayleigh-Taylor model (RT): This model describes breakup according to the Rayleigh-Taylor instabilities. Instability occurs when a drop rapidly decelerates due to drag. If the scaled wavelength of the parcel is smaller than the droplet diameter this model assumes that RT waves are increasing. If the RT waves have been increasing for a sufficient time, the droplet will break up. Instead of creating additional parcels, in RT breakup the parcel radius and the temperature and species mass fractions of the contained drops are augmented.

KH-RT model: This model is combination of KH and RT model. In this combined model the KH model is applied to the drop from the start of injection to vaporization while RT model is applied once the drop has reached the breakup length, L_b, which is calculated from the user-specified Model breakup length constant, $C_{bl.}$

$$L_b = C_{bl}\sqrt{\frac{\rho_1}{\rho_g}}d_o \qquad (2.2)$$

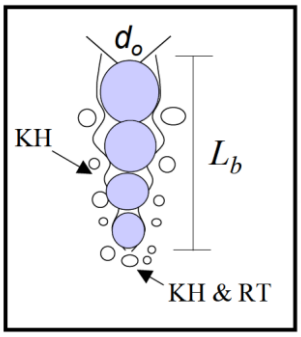

Figure 2.11 Schematic of the KH-RT spray breakup model [30]

Note that liquid blobs are injected with a diameter equal to that of the injector nozzle. In addition, the KH breakup mechanism is applied to a droplet throughout its lifetime, while the RT mechanism is only initiated once the drop reaches a characteristic distance, L_b, from the injector. In the KH wave model, atomization is treated using stability analysis for liquid fuel jets. The breakup of injected blobs and further resulting drops of radius r_0 is calculated by assuming that the drop radius is proportional to the wavelength of the fastest growing unstable surface wave Λ_{KH}.It is calculated as:

$$r = B_0 \Lambda_{KH} \tag{2.3}$$

where B_0 is a model constant. The droplet size, and its change of radius is calculated by:

$$\frac{d_{r_0}}{d_t} = -\frac{(r_0 - r)}{\tau_{KH}} \tag{2.4}$$

where the breakup time constant,τ_{KH} is calculated as:

$$\tau_{KH} = \frac{3.726 B_1 r_0}{\Lambda_{KH} \Omega_{KH}} \tag{2.5}$$

and the maximum growth rates Ω_{KH} and corresponding wavelengths Λ_{KH} have been simplified and defined as follows,

$$\Omega_{KH}\left(\frac{\rho_l a^3}{\sigma}\right) = \frac{0.34 + 0.38We_g^{1.5}}{(1+z)(1+1.4T^{0.6})} \tag{2.6}$$

and

$$\frac{\Lambda_{KH}}{a} = 9.02\ \frac{(1+0.45Z^{0.5})(1+0.4T^{0.7})}{(We_g{}^{1.67})^{0.6}} \tag{2.7}$$

where:

$$Z = \frac{We_l{}^{0.5}}{Re_l}\ , T = We_g{}^{0.5}, We_l = \frac{\rho_l U^2 a}{\sigma}$$
$$We_g = \frac{\rho_g U^2 a}{\sigma}\ , Re_l = \frac{Ua}{v_l} \tag{2.8}$$

The present RT mechanism formulation includes viscosity variations in the growth rate equation:

$$\omega_{RT} = -k_{RT}^2\left(\frac{\mu_l + \mu_g}{\rho_l + \rho_g}\right) + \sqrt{k_{RT}\left(\frac{\rho_l - \rho_g}{\rho_l - \rho_g}\right)a - \frac{k_{RT}^3\sigma}{(\rho_l + \rho_g)} + k_{RT}^4(\frac{\mu_l + \mu_g}{\rho_l + \rho_g})^2} \tag{2.9}$$

where k_{RT} is the wavenumber,μ_l is the liquid viscosity, μ_g is the gas viscosity, $\rho_l$is the liquid density, ρ_g the gas density, a is the deceleration of the drop, and σ is the liquid surface tension. The wave number corresponding to the maximum growth rate $K_{RT} = \frac{2\pi}{\Lambda_{RT}}$ is calculated through a bisection method with equation 2.9. The value is updated to calculate the maximum growth rate Ω_{RT}. The predicted RT model drop size is then expressed as:

$$r_{RT} = C_{RT}\Lambda_{KH} \tag{2.10}$$

where C_{RT} is the model constant, and Λ_{KH} is the predicted RT wavelength.

The No Time Counter (NTC) collision model of Schmidt and Rutland 2000 [42] was used in the present work. The outcome of a collision is predicted to be bouncing, stretching separation, reflexive separation, or coalescence, and was simulated based on the model of Post and Abraham 2002, [43].

Mono-component evaporation model of Amsden et al. 1989 [19] was used in the present calculations. The evaporation model was based on a Frossling correlation, which calculates the time change rate of drop radius based on the laminar mass diffusivity of the fuel vapor, the mass transfer, and the Sherwood numbers. The droplets were assumed to be fully mixed, with no gradient of temperature or component mass fraction inside of the droplet. Drop radius is determined from the mass rate of change due to evaporation or condensation equation:

$$\frac{d}{dt}r^2 = \frac{\rho_v}{\rho_d} D_v B_d Sh_d \tag{2.11}$$

where D_v is the vapor diffusivity in the gas and it is determined from the empirical Frossling correlation, $\rho_v D_v = D_1 \breve{T}^{D_2}$ having D_1 and D_2 as constants and $\breve{T}$. The Spalding mass transfer number is used to define,

$$B_d = (Y_v^* - Y_v)/(1 - Y_v^*) \tag{2.12}$$

and $Y_v = \rho_v/\rho_g$ is the vapor mass fraction, and Y_v^* is the vapor mass fraction on the drop surface calculated assuming equilibrium conditions and invoking the Clayperon thermodynamic equation,

$$Y_v^*(T_d) = \left[1 + \frac{MW_s}{MW_v}\left(\frac{p_g}{p_v(T_d)} - 1\right)\right]^{-1} \tag{2.13}$$

The molecular weights are denoted as MW_s, for the surrounding gas, and MW_v for the vapor. The equilibrium vapor pressure is denoted as, (T_d) and p_g is the gas pressure.

The Sherwood number is denoted as:

$$Sh_d = \left(2.0 + 0.6Re_d^{1/2}Sc_d^{1/3}\right)ln\frac{1 + B_d}{B_d} \tag{2.14}$$

where the droplet Schmidt number is defined as,

$$Sc_d = \frac{\mu(\breve{T})}{\rho_g D_g(\breve{T})} \tag{2.15}$$

The Raoult's law [44] was utilized in the present modeling to correlate the vapor mass fraction of the component over the surface and its mole fraction in the condensed phase.

2.4 Turbulence Modeling

The following section will discuss what turbulence is, how it is important in combustion, and different types of turbulence modeling approaches used in the modern simulation world.

In fluid dynamics, turbulence or turbulent flow is a flow regime characterized by chaotic and stochastic property changes. This includes low momentum diffusion, high momentum convection, and rapid variation of pressure and velocity in space and time [45]. Turbulence is defined as the unsteady, aperiodic motion in which all three velocity components fluctuate, mixing matter, momentum, and energy. During combustion, turbulence corrugates and stretches the flame surface area on which reactions occur,

causing faster burning due to increased flame surface, and flame extinction due to overstretching of flame surface. The Reynolds number, Re, which is the ratio of inertial forces to viscous forces, quantifies the turbulence level in a system. The higher the Re, the more chaotic the turbulence. In IC engines, the flow is almost always turbulent.

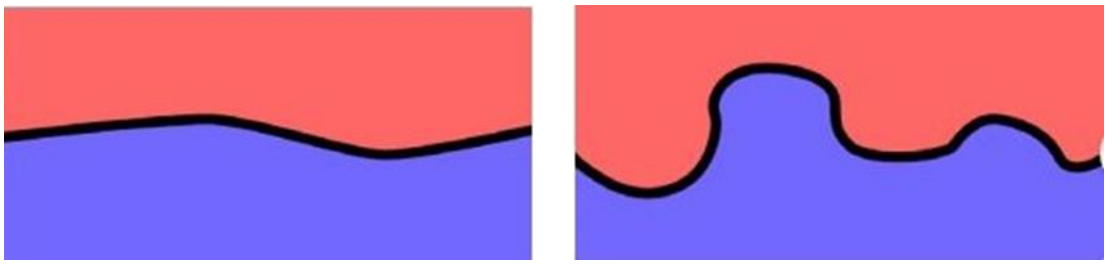

Figure 2.12 Laminar (left) and Turbulent (right) Flows [46]

In non-premixed engines, combustion depends on the rate of fuel-air mixing. Turbulence increases the rate of mixing. To resolve this enhanced mixing requires cells of order $1e^{-6}$ m. In premixed engines, by contrast, turbulence wrinkles the flame front, which increases the interface area and enhances the burn rate. To accurately model diffusion and predict the proper flame speed requires laminar flame thickness of the order of $1e^{-5}$ m in order to be resolved. These small length scales require the use of turbulence modeling techniques to simulate and predict flow accurately.

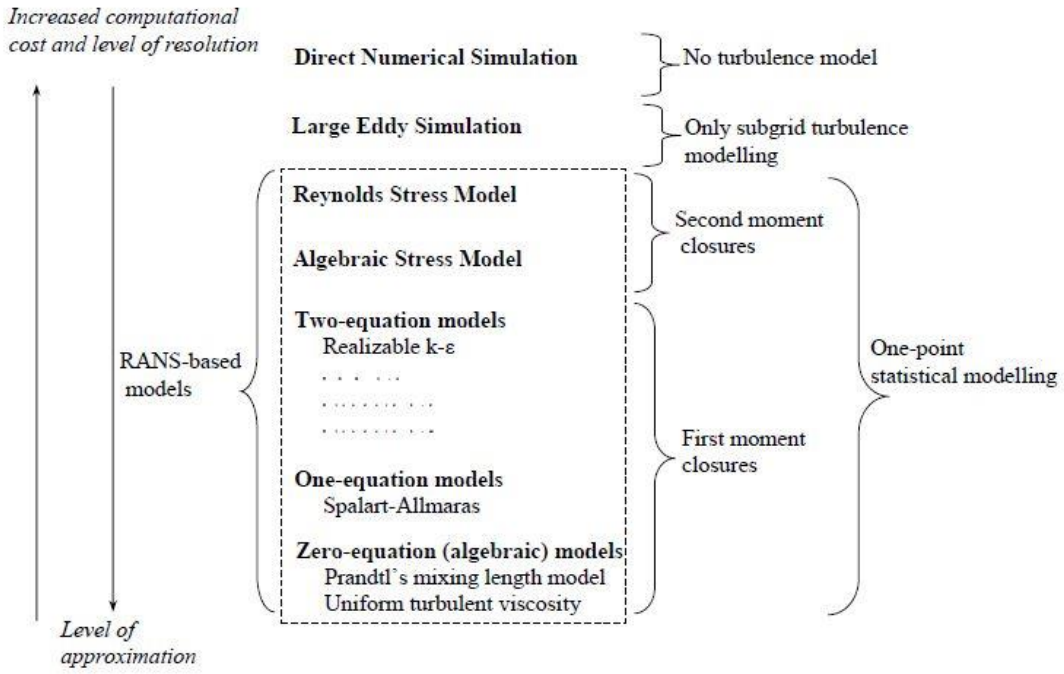

Figure 2.13 Schematic overview of turbulence modelling [45]

An overview of the different turbulence models is shown in Figure 2.13. It should be noted that there is a trade-off between model accuracy and computational cost. The fewer the approximations, the more computational power is required, and vice versa. For successful simulations, the most optimal combination of approximations and simulation should be selected. For example, for simple flows, good predictions can be obtained with simple turbulence models such as one-equation models. Even though the result may be less accurate for complex flows, such models will still indicate the effects of various design changes. Reducing the quality of the simulations can provide information about trends even as overall prediction accuracy is lessened. But with the rapid development of computers and CFD codes, advanced turbulence models with more levels of approximation are used in modern simulations of engineering applications.

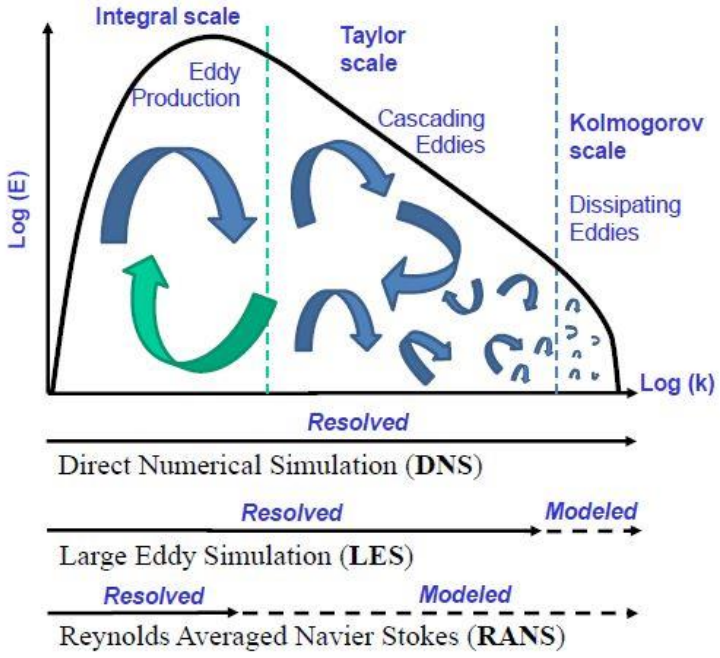

Figure 2.14 Length Scale Comparison of different turbulence models [45]

Due to spray inhomogeneities during multiphase mixing, modeling of the transients in the flow field is important. Mostly, coarse turbulence models are used in engine research to lessen the burden of the computational cost associated with the grid-resolution. Turbulence modeling is classified on its level of flow/grid resolution and its cost, as shown in Figure 2.14 DNS resolves all the length scales, LES resolves the anisotropic length scales (Integral scale and Taylor Scale) while modeling the isotropic/dissipation scales (Kolmogorov scale), and Reynolds Average Navier Stokes (RANS) that is based on ensemble averaging of the governing equations resolves only integral scale while modelling Taylor and Kolmogorov scales.

LES solves equations for a filtered time-dependent velocity field that represents large-scale turbulence motion. There are two classes of LES models - Zero-equation models: do not solve any additional transport equations, Zero-equation models available - Upwind (implicit) LES - Smagorinsky - Dynamic Smagorinsky. And One-equation models: solve an additional transport equation for sub-grid kinetic energy and One-equation models - Viscous one-equation - Dynamic structure - Consistent dynamic structure. RANS solve equations for an ensemble-averaged velocity field and the magnitude of the turbulent fluctuations. Standard k-ε, RNG k-ε Rapid Distortion RNG k-ε, Realizable k-ε, Standard k-ω 1998, Standard k-ω 2006, k-ω SST. The Large Eddy Simulation (LES) and RANS of turbulent model is used in spray combustion simulation. One equation dynamic structure of Pomraning [47] is utilized for LES turbulent modeling as it includes transport equation for k as well as works well with combustion models and spray models that require k. Also standard RNG k-ε [48], is used for RANS modeling as it accounts for more scales of motion. It performs better for separated flows and swirling flows.

2.5 Combustion Chemistry Modeling

This section will discuss two different types of combustion models used to solve the detailed chemistry. First, general overview of look-up table generation method, methodology and implementation of Dacolt PSR+PDF (Tabkin) tabulated model in CONVERGE are explained, and lastly, the different equations used to solve variables and reaction rates are presented. The second model presented is direct integration SAGE chemistry solver and the different techniques used to expedite the simulation time are explained.

2.5.1 Tabulated Chemistry Solver: FGM

First combustion chemistry solver used in this thesis is the Dacolt PSR+PDF [49] tabulated chemistry model which is a combination of flamelet generated manifolds (FGM) technique and presumed-Probability Density Function (PDF) turbulence chemistry interaction modeling, it parameterizes thermochemical states in flamelets by mixture fraction and reaction progress. It generates look-up table which is read by the CFD code at the start of the simulation. The look-up table generation has three steps [50]:

1) Preprocessing of the textual input files.
2) PSR simulations.
3) Post processing of the outputs.

An overview of the generation of the look-up table is presented below in Figure 2.15:

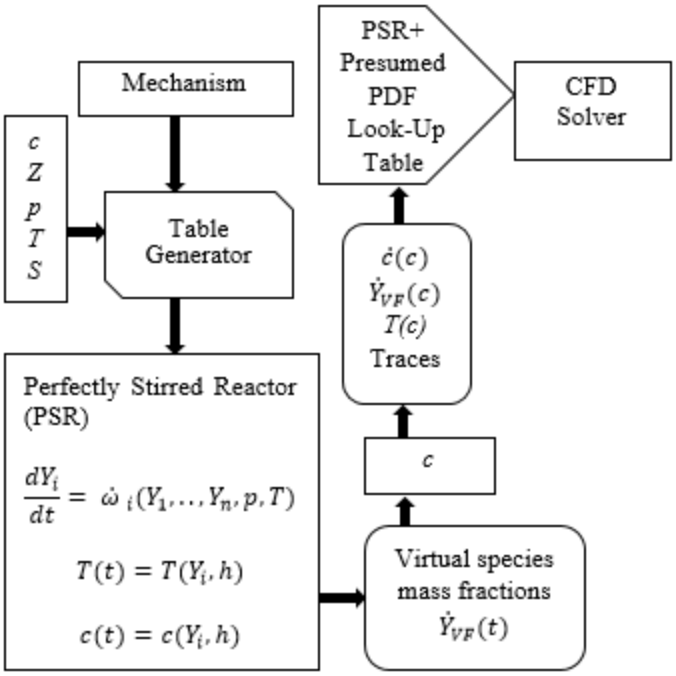

Figure 2.15 Generation of the chemistry table using PSR+ presumed PDF

As Figure 2.15 shows, the input variables are progress variable (*c*), mixture fraction (*Z*), ambient pressure (*p*), initial temperature (*T*), and mixture fraction segregation (*S*). Initial composition of species are computed, and perfectly stirred reactor (PSR) model are used for generating the table by using fuel mechanism. The n-dodecane mechanism of [22] with 85 species and 266 reactions is used in current work. In the last step for each variable ψ, PDF average $\widetilde{\psi}$ is computed for each mean mixture fraction Zm and segregation S using the following equation:

$$\widetilde{\psi} = \int_0^1 \psi(z) P(z; Z_m, S) dz \qquad (2.16)$$

The value of $S = 0$ corresponds to using a delta-function for the PDF *P(Z)*. For values of *S>0, P(Z)* is the beta-PDF with mean Z_m and normalized variance (segregation) *S*. Finally,

all variables are stored in the look-up table which is read by CFD code before the start of the simulation.

The current tabulated chemistry methodology can be described in three steps:

1) The combustion chemistry is pre-computed and relevant data is stored in a multi-dimensional database (look-up table). Perfectly Stirred Reactors (PSR) model will be utilized to compute the scalar as will be discussed. In PSR model, the simulation is carried out at constant pressure with known initial composition and temperature.

2) The look-up table will be read by the CFD code at the start of a simulation. Converge CFD commercial package is utilized in this thesis.

3) The combustion data is interpolated during the iterative calculation steps of the CFD solver.

Three scalar equations are solved using FGM model, namely, progress variable *c*, mean mixture fraction *Z* and mixture fraction variance Z_{var}. Progress variable *c* governs the advancement of ignition and flame development and it describes how the reaction progresses from fresh to burnt gas. The transport equation for the normalized mean progress variable is:

$$\frac{\partial}{\partial t}(\overline{\rho}\tilde{c}) + \frac{\partial}{\partial x_i}(\overline{\rho}\tilde{u}_i\tilde{c}) = \frac{\partial}{\partial x_i}\left[\overline{\rho}(D + D_T)\frac{\partial \tilde{c}}{\partial x_i}\right] + \overline{\rho}\,\overline{\dot{\omega}}_c \qquad (2.17)$$

Over lines denote general filtering and tildes denote the progress variable. In the equation (2.17) $\overline{\rho}, \tilde{c}, \tilde{u}_i, D, D_T, \overline{\dot{\omega}}_c$ are density, progress variable, velocity of species *i*, laminar diffusion coefficient, turbulent diffusion coefficient and progress variable source term respectively.

The normalized progress variable is given by:

$$c = \frac{Y_C}{Y_C^{EQ}} \tag{2.18}$$

Y_C, Y_C^{EQ} are mass fraction of species at given conditions and mass fraction of species at equilibrium respectively. In this thesis, a linear combination of species CO_2, CO, CH_4 and HO_2 are used for progress variable.

Mixture fraction is a conserved scalar which determines the process between fuel and air mixing. The transport equation for mixture fraction is:

$$\frac{\partial}{\partial t}\left(\overline{\rho}\tilde{Z}\right) + \frac{\partial}{\partial x_i}\left(\overline{\rho}\tilde{u}_i\tilde{Z}\right) = \frac{\partial}{\partial x_i}\left[\overline{\rho}(D + D_T)\frac{\partial \tilde{Z}}{\partial x_i}\right] + \overline{\dot{\omega}}_{vap} \tag{2.19}$$

Over lines denote general filtering and tildes denote mean mixture fraction. In equation (2.19) $\overline{\rho}, \tilde{z}, \tilde{u}_i\ D, \overline{\rho}, \tilde{z}, \tilde{u}_i, D, D_T, \overline{\dot{\omega}}_{vap}$ are density, mixture fraction, velocity of species *i*, laminar diffusion coefficient, turbulent diffusion coefficient and vaporization rate respectively.

The transport equation for mean mixture fraction variance $Z^{"}$:

$$\frac{\partial}{\partial t}\left(\overline{\rho}\widetilde{Z^{"2}}\right) + \frac{\partial}{\partial x_i}\left(\overline{\rho}\tilde{u}_i\widetilde{Z^{"2}}\right) = \frac{\partial}{\partial x_i}\left[\overline{\rho}(D + D_T)\frac{\partial \widetilde{Z^{"2}}}{\partial x_i}\right] + 2\overline{\rho}\ D_T\left[\frac{\partial \tilde{Z}}{\partial x_i}\right]^2 - \overline{\rho}\tilde{\chi}_Z \tag{2.20}$$

$\tilde{\chi}_Z$, scalar dissipation rate is calculated by:

$$\tilde{\chi}_Z = 2\frac{\varepsilon}{k}\widetilde{Z^{"2}} \tag{2.21}$$

Implementation of FGM combustion model simplifies the chemistry of all species into a virtual system which is solved using a single step chemistry. The virtual fuel created

consists of artificial species whose physical and thermochemical properties are the same as that of the fuel. A variable Y_{VF} called virtual fuel mass fraction is generated which allows imposing of mass fraction from the look up table as function of lookup coordinates $c, Z, S, S_Z, S_C, T_{FG}$ which are progress variable, mixture fraction, scaled variance, scaled mixture fraction variance, scaled progress variable variance and fresh gas temperature respectively. The rate of change of virtual fuel is calculated by:

$$\dot{Y}_{VF} = \frac{Y_{VF}(t + \Delta t) - Y_{VF}(t)}{\Delta t} \tag{2.22}$$

$$\dot{Y}_{VF} = \frac{Y_{VF}(c(t + \Delta t), coords) - Y_{VF}(c(t), coords)}{\Delta t} \tag{2.23}$$

where Δt is the local time-step and is typically smaller than the CFD time-step by a factor of 10. In the final step of the approach, chemical heat source term is computed.

$$\dot{\omega}_{HR} = \rho \sum_i \dot{Y}_i h_i \tag{2.24}$$

where $\dot{\omega}_{HR}, \rho, \dot{Y}_i, h_i$ are, species change rates, density, mass fraction, and partial enthalpies of species *i* respectively.

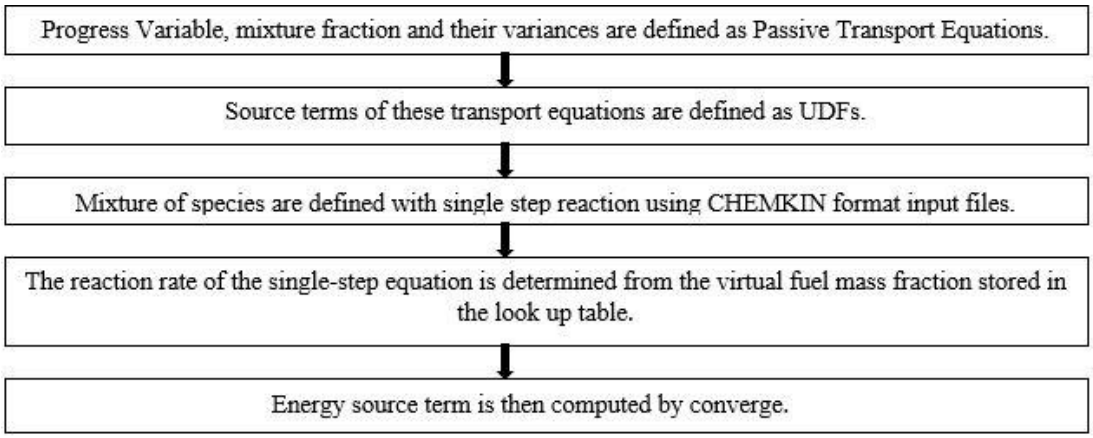

Figure 2.16 Implementation of the Tabkin model in CONVERGE [51]

2.5.2 Direct Integration Chemistry Solver: SAGE

SAGE solver models detailed chemical kinetics in combustion simulations with a set of CHEMKIN formatted input files. It solves initial value problems for ordinary differential equation (ODE) systems and calculates the reaction rates for each elementary reaction, while the CFD solver solves the transport equations [52]. Forward reaction rates are calculated using Arrhenius formula, while reverse reaction rates use equilibrium coefficients, which are determined using thermodynamic properties. The governing equations for mass and energy conservation for a computational cell are solved using forward reaction rate coefficient (k_{fr}), reverse reaction rate coefficient (k_{rr}), equilibrium constant coefficient (k_{cr}), and change in entropy and enthalpy. SAGE solves the system rate of equations while CONVERGE updates the species concentration at each computational time step and for each species, and using the computed species concentration calculations converged cell temperature is updated. In SAGE, there are ways to expedite the simulation [30]. The first method sets a limit to previous cell temperature, and if the limit is met, skips the re-calculations for that range. The second method uses Jacobin matrix calculations and

the third method is multizone in which the detailed chemistry is solved in zones, i.e. groups of cells, with similar thermodynamic properties. None of the above methods are used in this thesis instead a minimum cell temperature T_{cut} is specified below which kinetics are not solved. The cutoff temperature was set to 400 K in this research work.

2.6 Pressure Correction Triangulation Theory

This section will discuss the mathematical model used to correct pressure rise timing. The pressure triangulation correlation used in this thesis was developed and validated experimentally by Lillo [53], which used speed of sound at chamber condition and the distance between location of autoignition and the sensor to correct pressure rise.

2.6.1 Numerical Methodology

The ignition follows the path of fuel vaporization and air fuel mixing followed by low temperature (first stage) heat release and high temperature heat release. This transition to high temperature combustion represents the start of major heat release combustion and the time lag between this transition is called ignition delay in diesel engine. Chemical heat release events create propagating pressure waves that are detectable by sensors [54-55].

To calculate the heat release and ignition delay time of diesel engines, pressure measurements play a vital role. There has been extensive study on the correction of pressure rise using speed of sound and location of auto ignition, but there has been not been conclusive relations for prediction of pressure based ignition delay. The time delay between the creation of pressure wave during heat release events and detection by the pressure transducer is dependent on gas properties and the distance between them. A few studies took this into account but neglected the speed sound correction [56-57].

Higgnis and Siebers [58] used chemillumence and measured pressure in a constant volume chamber by applying the speed of sound corrections to measure data for diesel engines ignition delays. They used distance between the penetrating jet and pressure transducer to make the correction, shifting the corrected pressure reading by 0.1 ms of the time of ignition and thus aligning the pressure rise in the vessel detected using a high sensitive photodiode, although in this case a coarse data sampling resolution was used (28 micro seconds). To determine pressure based ignition delay, the foremost step is to measure the pressure rise. Usually, pressure based ignition delay is said to be achieved when the pressure rises to 1 kPa or 3 kPa, at which point a reading of time is taken.

The pressure sensors are located at the lower corners of the constant volume combustion chamber and at a distance from the region of high temperature chemistry in a constant volume chamber at the Sandia National Lab, which is modeled in the current work and will be explained with more detail. A pressure wave will travel by speed of sound from the location(s) of combustion to reach the sensors. Therefore, what is measured at the sensor location has actually happened sometime before at the location of combustion. Lillo [53] has explained briefly this phenomenon and used it to correlate the experimental results which were published on the ECN website. The current work uses the same methodology, which accounts for the speed of sound when determining the timing of the predicted pressure rise in the combustion chamber.

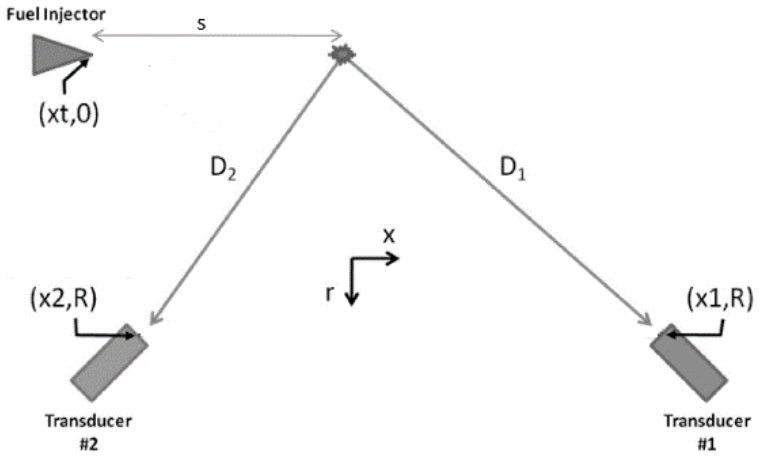

Figure 2.17 Ignition location determination using two pressure sensors [53] Distance (*s*) shows the position of combustion where the pressure waves travel

To correlate the timing, the pressure is measured at two different locations in the combustion chamber as shown in Figure 2.17 . These two data readings come from the same source (auto-ignition) in the combustion chamber. These two data readings are not equal since the location of measurements are different (and so the distance between the source and the measurement sensors are different) as shown in Figure 2.17 . By using this time delay, the location of combustion will be determined and the data will be correlated to measure the actual timing of pressure rise and pressure-based ignition delay.

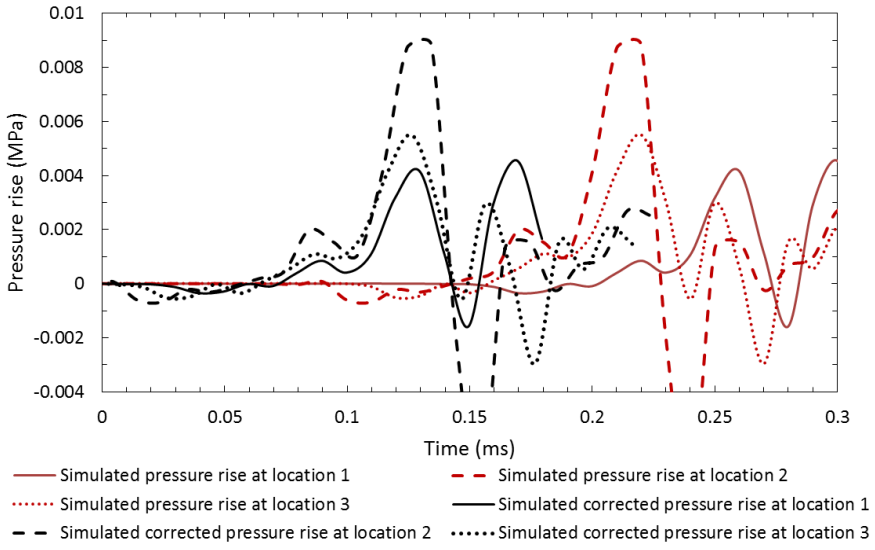

Figure 2.18 The uncorrected and corrected pressure rise at three different locations: location #1 (0, 0.053, 0.0806), location#2: (0, 0.05303, 0) and location#3 (0, 0.5303, 0.04) with respect to the injector; all dimensions are measured in meters. The initial temperature of combustion chamber is 1200 K. SAGE and LES were utilized for pressure-rise modeling

To measure pressure in the combustion chamber, pressure transducers were used in both experimental and simulation set up. The location of ignition can be determined more accurately by using pressure sensors but cost also plays an important role. Three sensors were used in this thesis to achieve more simulation accuracy as shown in figure 2.15.

Upon occurrence of ignition at some (x, r), a pressure wave propagates throughout the control volume. The distance ignition pressure-wave travels to reach sensor, i.e. D_1, and D_2 can be predicted by knowing the delay between the two sensors, speed of sound, and coordinates of each sensor according to the following equation:

$$\Delta t = t_1 - t_2 = \frac{D_2 - D_1}{c} = \frac{[((s + x_t - x_2)^2 + R^2)^{0.5} - ((x_1 - x_t - s)^2 + R^2)^{0.5}]}{c} \quad (2.25)$$

The only unknown variable in Eq. 1 is (s) and can be determined easily. The assumptions behind the formula are that the speed of sound (c) is the same between the two transducers and autoignition location, and the combustion/autoignition is happening one point at a time. As discussed by Lillo [53] the error of this assumption in finding the location of combustion is small enough and within the accuracy of experimental measurements. The location of the combustion can be determined in three-dimensional space more accurately by adding one more sensor. The vessel pressure measurement shows a decrease in pressure during the cool-down period prior to fuel injection. The pressure rise caused by fuel spray combustion accounts for the difference between the measured pressure at combustion and the cool-down periods. Therefore, the present simulation was carried out in two steps: first by modeling the entire spray combustion and second by deactivating the spray and combustion models to simulate the pressure drop during the cool-down period.

The corrected and uncorrected pressure-rise at three different locations are shown in Figure 2.18 . The first and second peaks of three corrected pressure-rises are happening at the same timing, ~ 0.9 ms and 0.125 ms respectively. Only the first and/or second significant peak(s) with magnitude of higher than 1 kPa was used for pressure rise correction. The location of autoignition using described methodology at initial combustion chamber temperature of 1200 K is shown in Figure 2.19 . The resultant pressure rise (difference between two pressure rises) was compared with experimental data which is discussed in the results and discussions section of this thesis.

Figure 2.19 Temperature profile of combustion chamber1200 K and timing of 0.3 ms after start of injection utilizing SAGE and LES. The location of autoignition is shown by the green star

CHAPTER 3

3 RESULTS and DISCUSSIONS

3.1 Chapter Overview

The following chapter will discuss the results of the simulations. The data is presented via the following graphs and figures: pressure rise vs time at near wall and opposite to injector sensor, vapor penetrations, spray penetrations, temperature profiles, temperature rise, and total cell count. In all cases the results were in agreement with the experimental data. This section is divided into four subsections. First the dependency of Turbulent Spray Combustion Modeling on mesh resolution using Flamelet Generated Manifolds is studied, there after the effects of combustion models and the effects of turbulence models on spray behavior will be discussed and finally, the lift-off length using various models are investigated.

3.2 Mesh Size Investigation

The pressure rise at location of (0, 53, 80.6) mm respect to injector (0,0,0) which positioned opposite to the wall of injector is shown in Figure 3.1. The exact location of pressure sensor in experimental setup include uncertainties and is not clear for the simulations. As shown in Figure 3.1 and Figure 3.2, the pressure rise does not show meaningful dependency on mesh size.

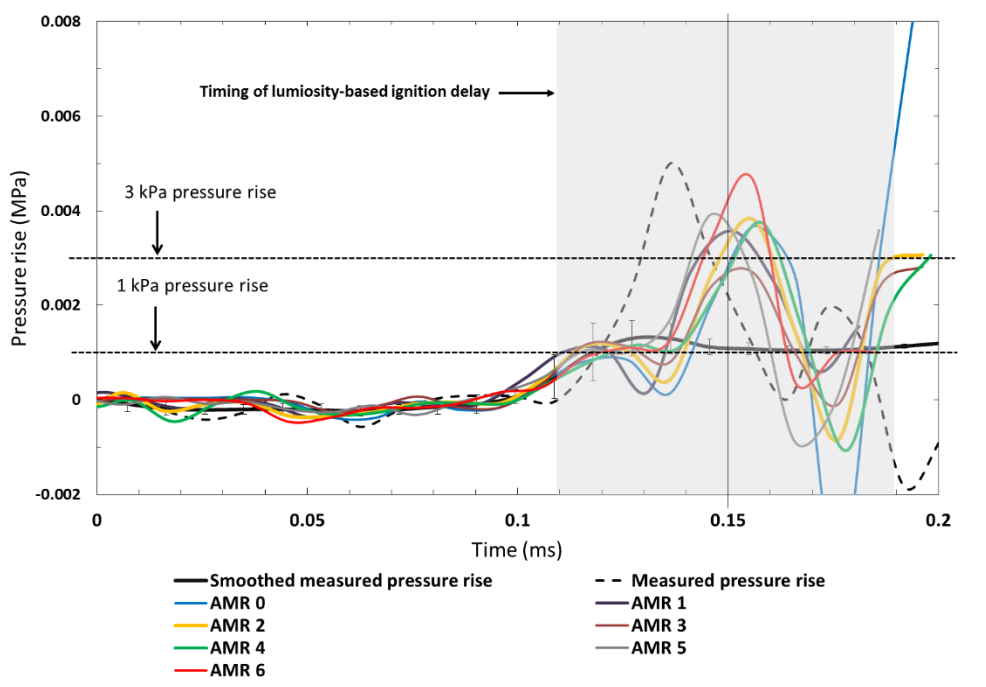

Figure 3.1 Corrected pressure-rise at location of transducer#1 using various mesh sizes at initial temperature of 1200 K in combustion chamber utilizing FGM and LES

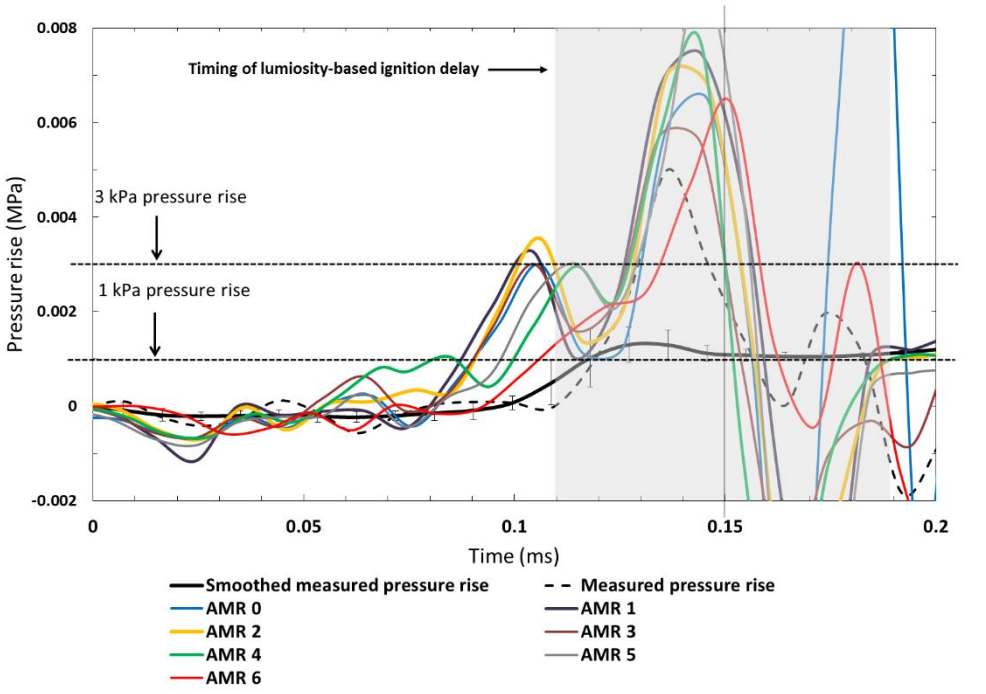

Figure 3.2 Corrected pressure-rise at location of transducer#2 using various mesh sizes at initial temperature of 1200 K in combustion chamber utilizing FGM and LES

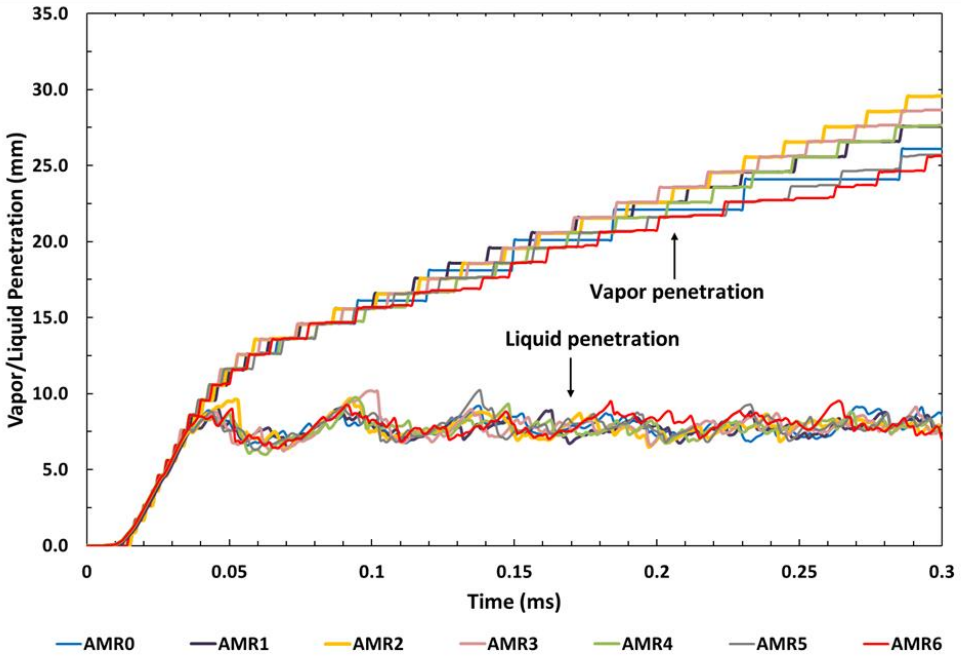

Figure 3.3 Liquid and vapor penetration using various mesh sizes at initial temperature of 1200 K in combustion chamber utilizing FGM and LES

Liquid and Vapor penetration profile is shown in Figure 3.3. As expected, the liquid penetration does not show dependency to mesh refinement despite using various mesh refinement methods since the liquid penetration length is less than the embedded mesh length (12 mm). Purposely 12 mm embedding length with mesh size of 0.031 mm was used for all the cases to eliminate one variable in the computational domain.

The dependency of vapor penetration to mesh refinement is distinguishable after 0.05 ms (or 12 mm) in Figure 3.3 . The difference between vapor penetrations using various mesh sizes could be clearly observed at around 0.3 ms. The onset of high temperature combustion is of interest in current research and the timing of start of high temperature combustion is about 0.11 ms as shown previously by gray area in Figure 3.1 In addition, the difference between vapor penetrations various mesh refinements are small (less than

5% variation respect to averaged value of all the simulations) till 0.15 ms. Therefore, the effect of vapor penetration on pressure rise or high temperature combustion using various mesh size could be neglected.

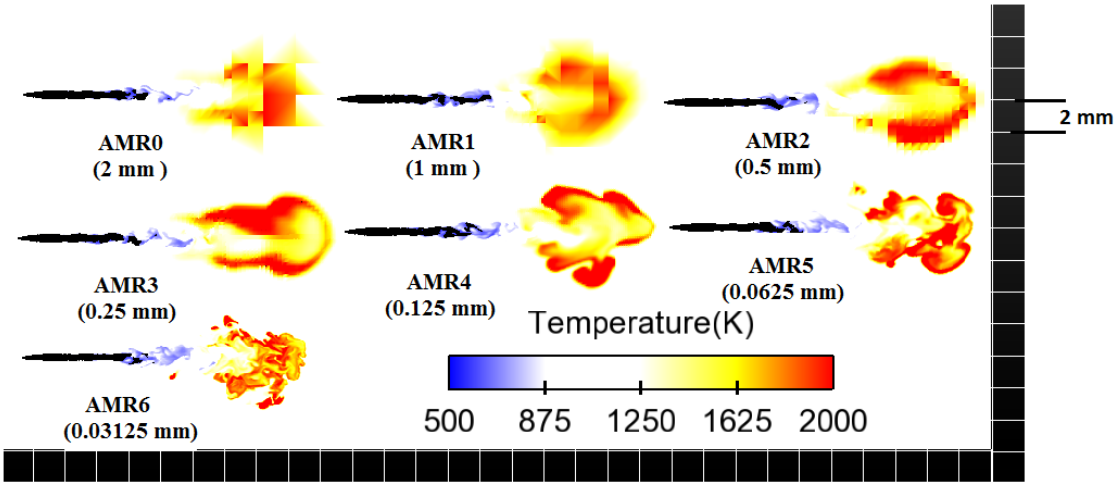

Figure 3.4 Temperature profiles at 0.16 ms after start of injection using various mesh sizes. The black dots represent liquid droplets

The temperature profile for various mesh sizes are shown in Figure 3.4. More flame structures are captured using finer mesh but as shown before, the outcome (pressure rise) is independent of mesh size.

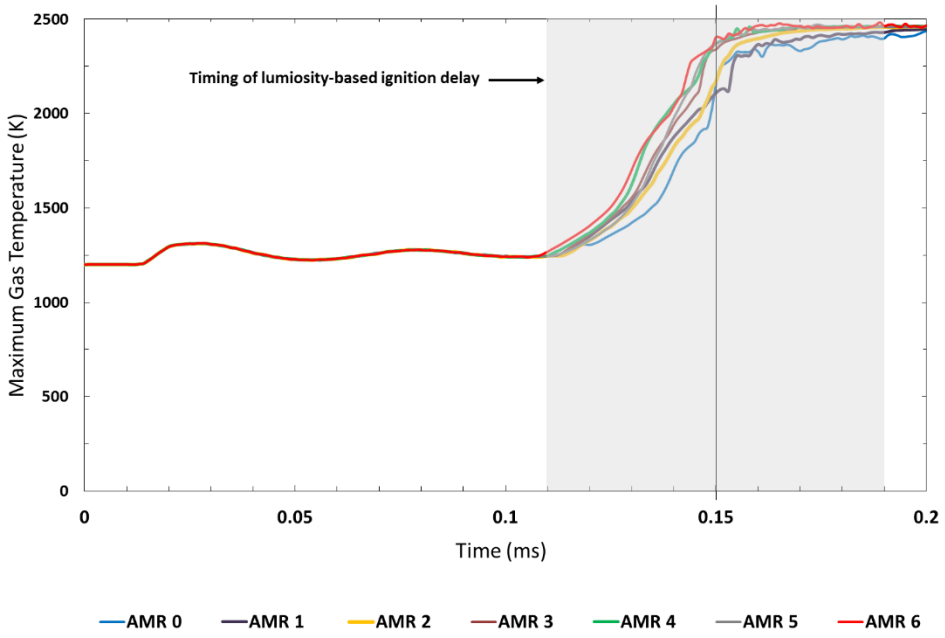

Figure 3.5 Temperature rise using various mesh sizes utilizing FGM and LES

Maximum temperature rise is shown in Figure 3.5 . The difference between the onset of temperature rise using various mesh sizes are less than 5% and in agreement with experimental data

3.3 Effects of combustion model on spray behavior

The second objective of this thesis was to evaluate the performance of FGM (or tabulated chemistry) versus DIC (or SAGE). Therefore, the turbulent spray combustion of n-dodecane was modeled at four initial temperatures of 900 K, 1000 K, 1100 K and 1200 K and surrounding gas density of 22.8 kg/m^3. LES turbulence model was used for modeling.

The maximum gas temperatures at various temperatures and pressures in combustion chamber are shown in Figure 3.6 to Figure 3.9 . The gas temperature starts

rising earlier using FGM with respect to SAGE at two initial gas temperatures of 900 K and 1000 K. Both models behave the same at initial gas temperature of 1100 K. At 1200 K, FGM predicts an earlier temperature rise with respect to SAGE. The numerical reason behind this behavior is still under investigation.

Maximum gas temperature in combustion chamber reaches temperature of 2000 K or higher within the range of measured OH* luminosity timing (gray area in the graphs) for all the cases. Basically, both models predict the timing of luminosity-based ignition delay and spray to spray variations within acceptable error and uncertainty margins.

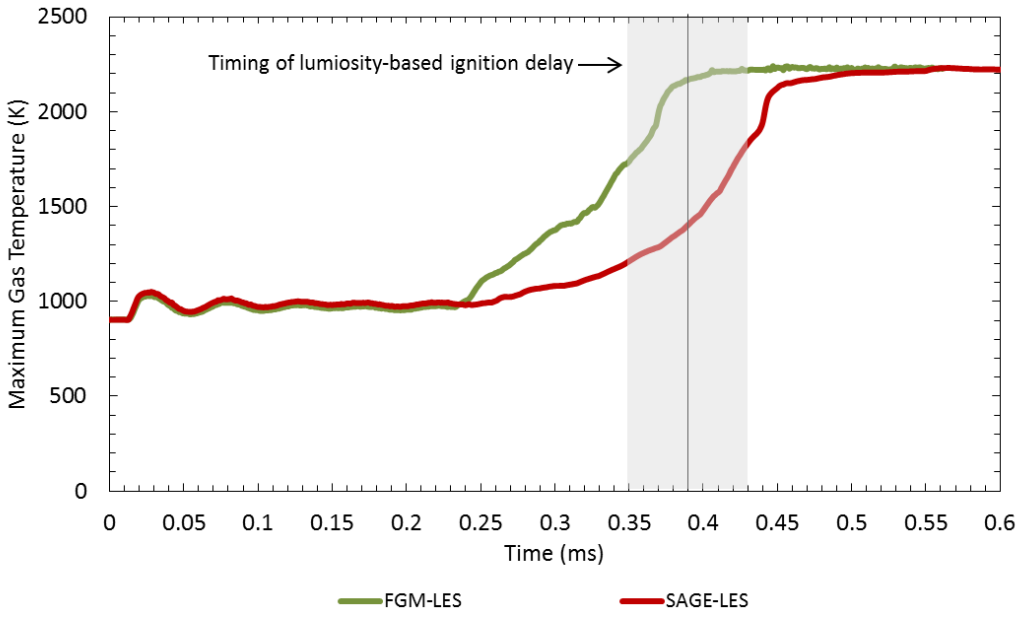

Figure 3.6 Maximum gas temperature at surrounding initial gas temperature of 900 K and pressure of 59.35 bar

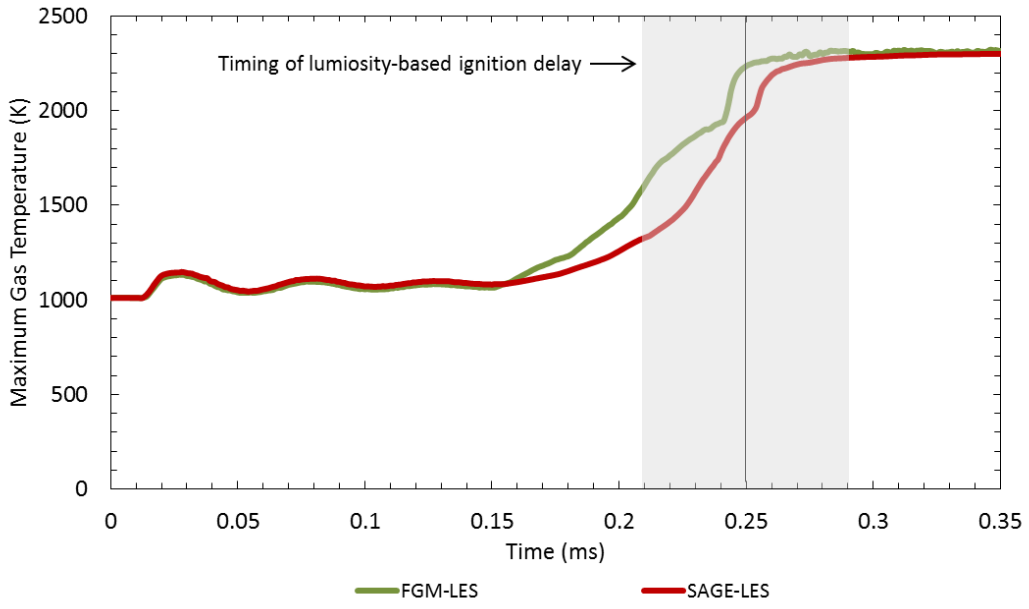

Figure 3.7 Maximum gas temperature at surrounding initial gas temperature of 1000 K and pressure of 66.20 bar

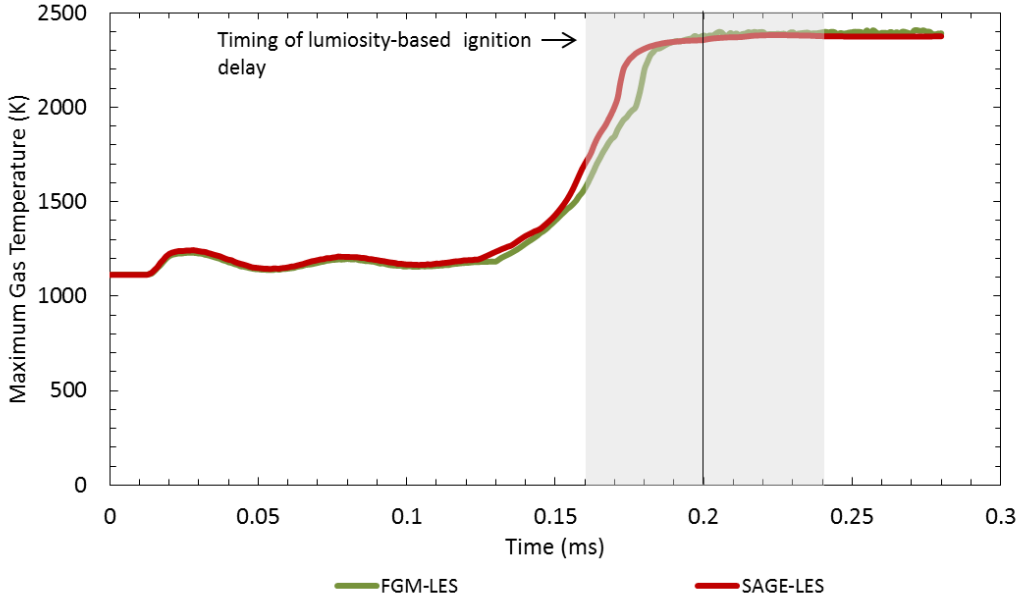

Figure 3.8 . Maximum gas temperature at surrounding initial gas temperature of 1100 K and pressure of 73.0 bar

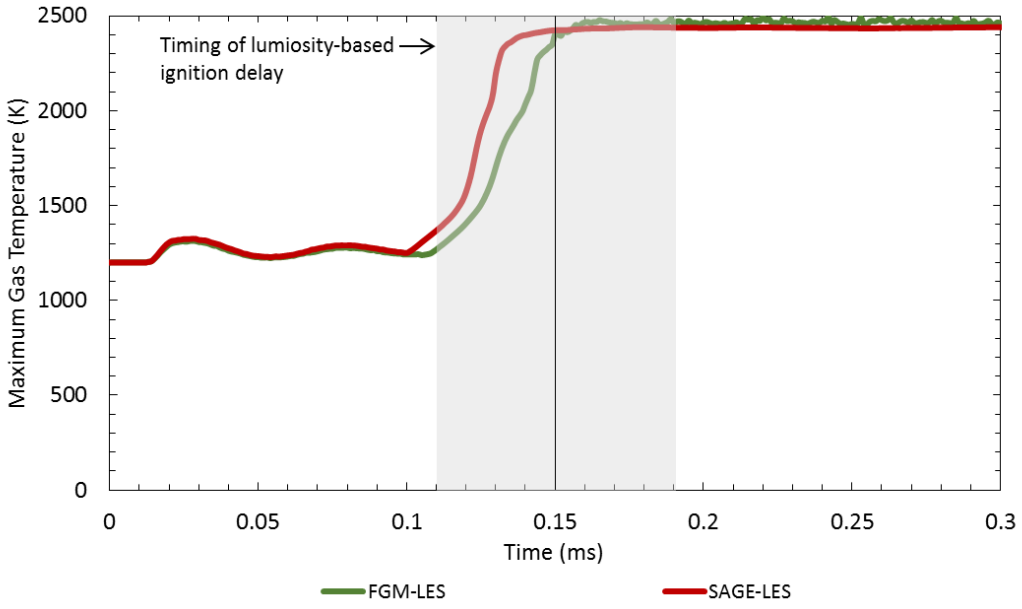

Figure 3.9 Maximum gas temperature at surrounding initial gas temperature of 1200 K and pressure of 79.4 bar

The corrected pressure-rises at various initial gas temperatures using two combustion models are shown in Figure 3.10 to 3.13. Predicted corrected-pressure rises behave differently using two combustion models, but significant rises of pressure are observed at timing of measured luminosity of OH* for all of the cases. The corrected pressure-rise and maximum temperature behave the same way as expected, e.g. at initial gas temperature of 900 K using the FGM combustion model, pressure and temperature rise simultaneously at approximately 0.25 ms. It is one of the noticeable trend in Figures 3.6 – 3.13, which show that corrected-pressure and temperature start rising at the same exact time, which demonstrates the accuracy of pressure triangulation methodology.

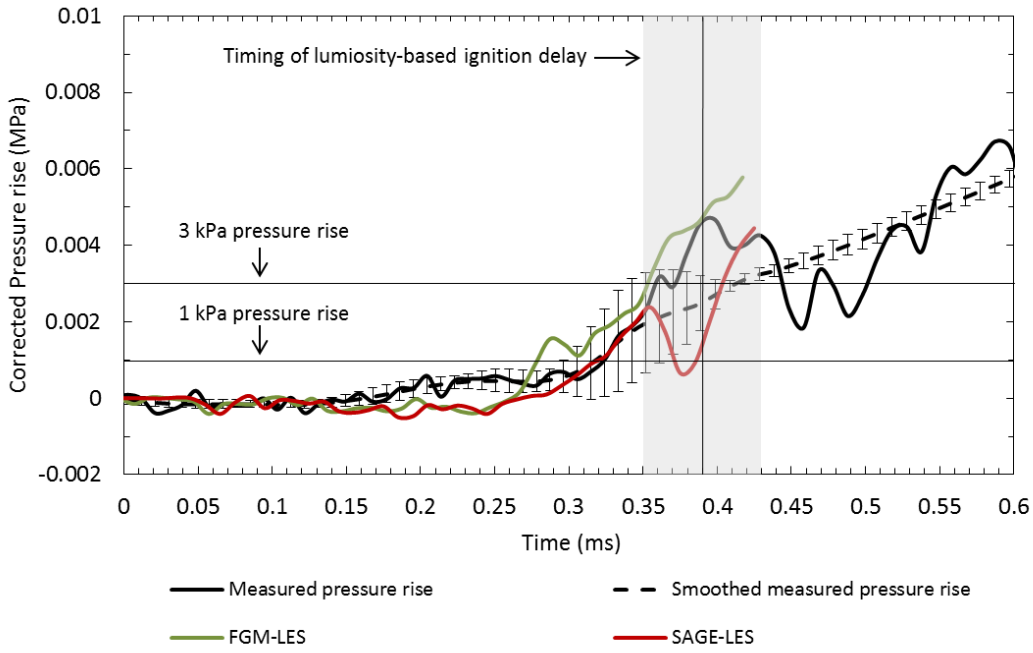

Figure 3.10 Corrected pressure-rise and measured data at surrounding initial gas temperature of 900 K and pressure of 59.35 bar

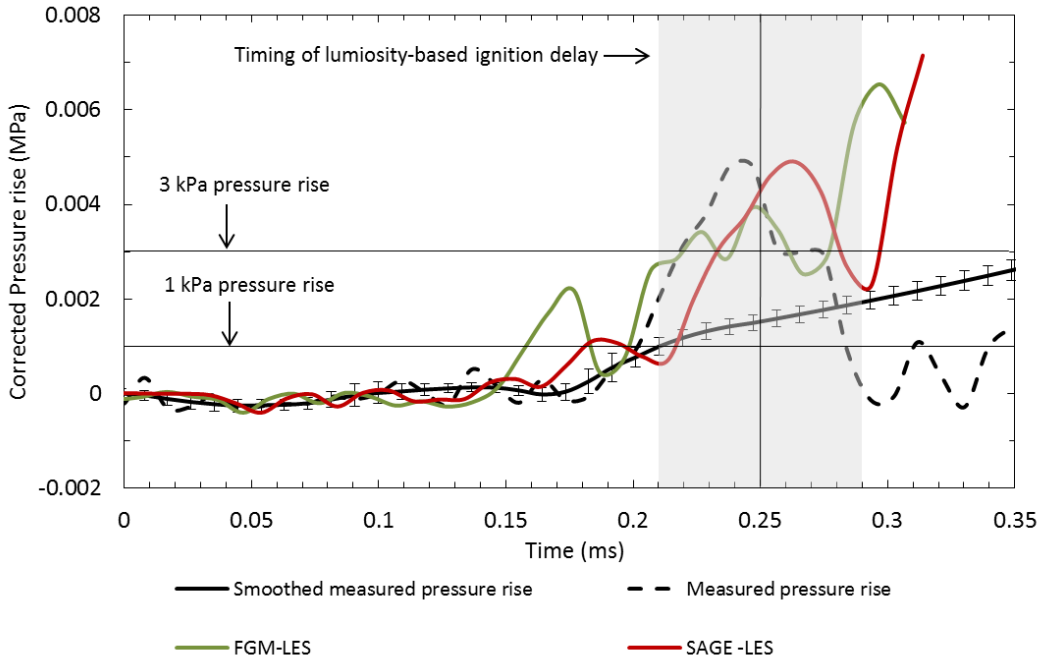

Figure 3.11 Corrected pressure-rise and measured data at surrounding initial gas temperature of 1000 K and pressure of 66.20 bar

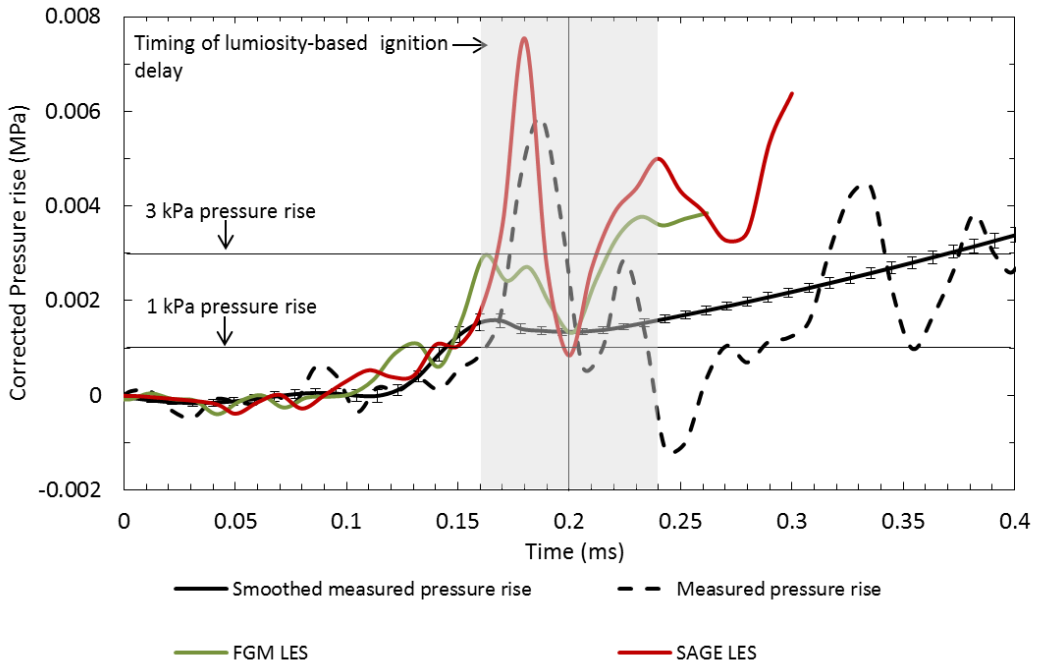

Figure 3.12 Corrected pressure-rise and measured data at surrounding initial gas temperature of 1100 K and pressure of 73 bar

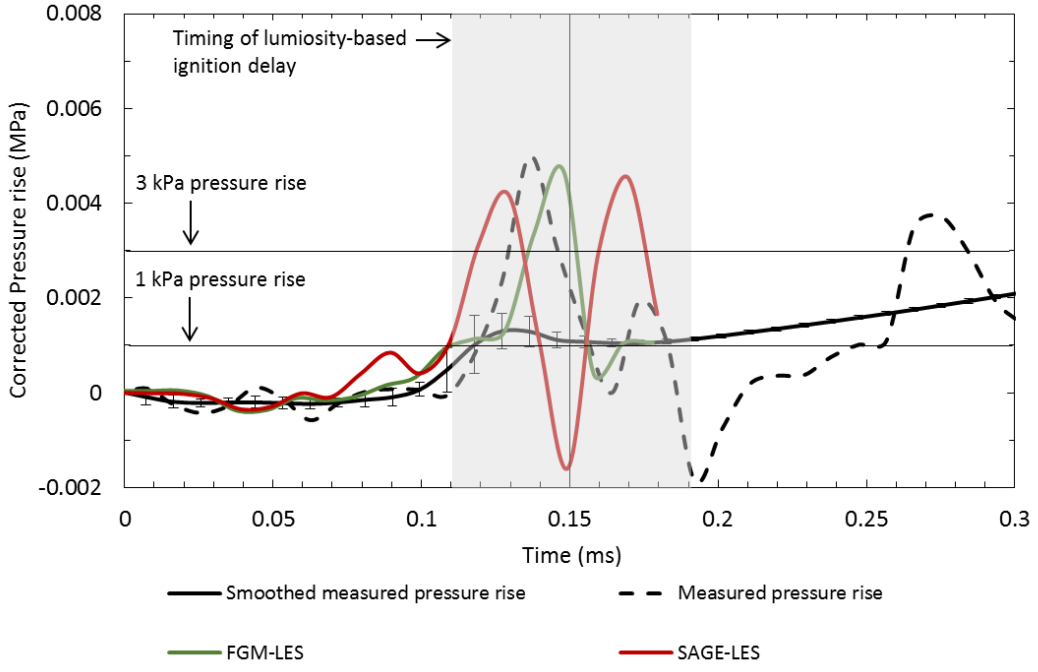

Figure 3.13 Corrected pressure-rise and measured data at surrounding initial gas temperature of 1200 K and pressure of 79.4 bar

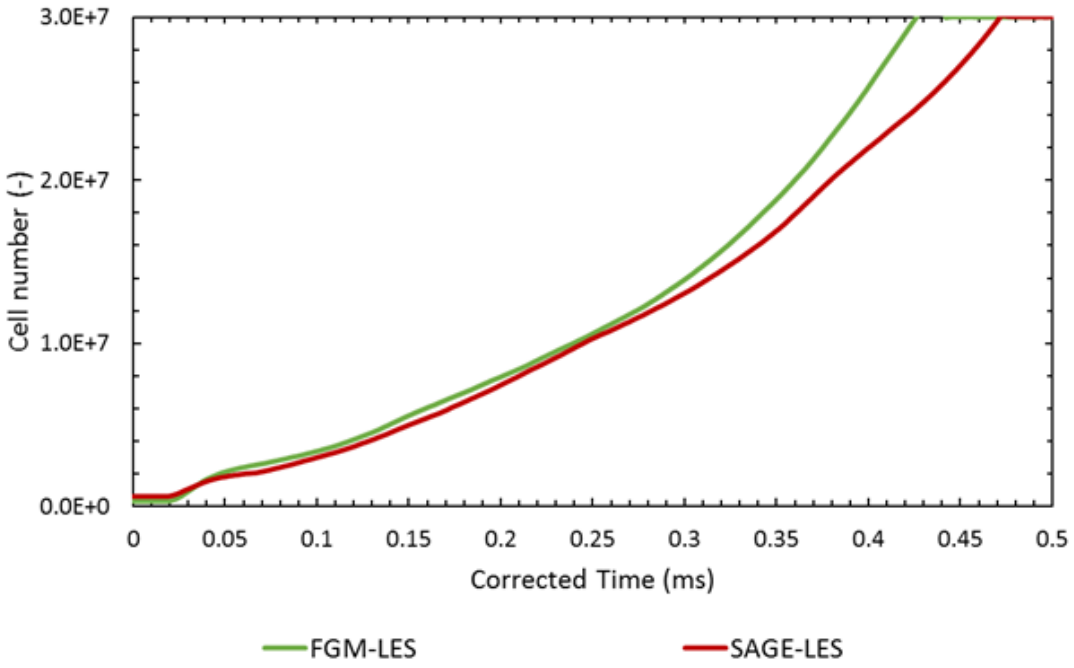

Figure 3.14 Total cell numbers at surrounding initial gas temperature of 900 K and pressure of 59.35 bar

As discussed briefly, adaptive mesh refinement (AMR) with maximum mesh number of 30 million was utilized in the current work. The total number of generated mesh using both models during simulation at initial gas temperature of 900 K are shown in Figure 3.14. Both models behave the same way, which shows that the two models have similar sub-grid velocity and temperature conditions.

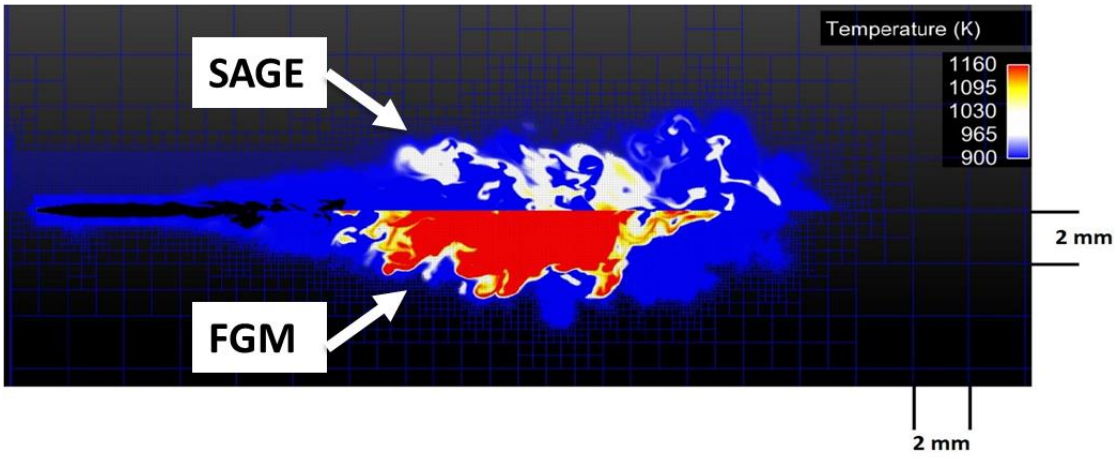

Figure 3.15 Temperature profiles at 900 K using two combustion models at 0.35 ms after start of injection

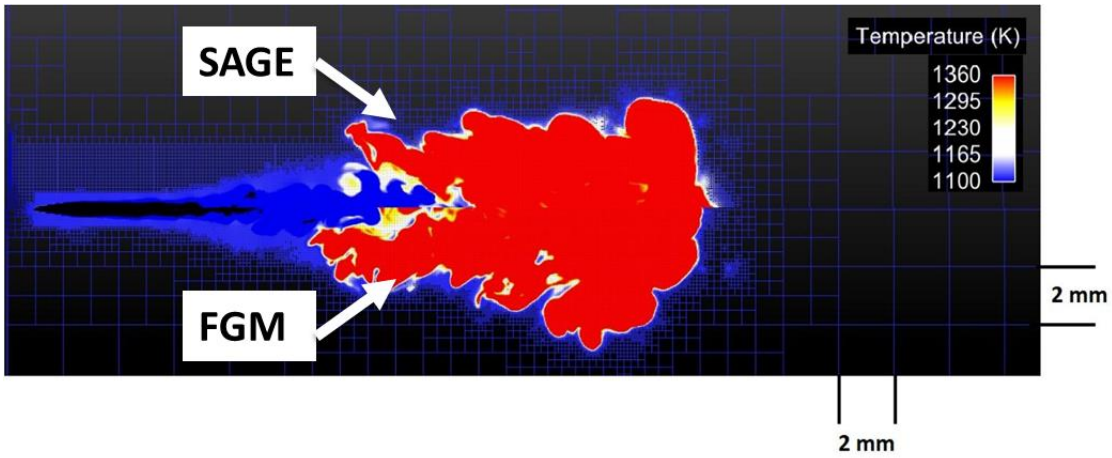

Figure 3.16 Temperature profiles at 1100 K using two combustion models at 0.30 ms after start of injection

The temperature profiles at two initial gas temperatures of 900 K and 1100 K are shown in Figure 3.15 and 3.16. As shown previously in Figure 3.6, the maximum gas temperature at 0.35 ms is about 1200 K using the SAGE model and 1700 K using the FGM model. This higher maximum gas temperature using FGM with respect to SAGE can also be observed in Figure 3.15. After passing the initial phase of combustion, where the maximum gas temperature is below 2000 K and the turbulent spray combustion has a transient behavior, both the FGM and SAGE models predict very similar temperature profiles as shown in Figure 3.16.

3.4 Turbulence model

The effect of two turbulence models, Dynamic-Structure-LES and RNG-RANS, on maximum gas temperature, pressure-rise and number of meshes at initial gas temperature of 1200 K are shown in Figures 3.17 to 3.21. Combustion temperature and pressure start rising earlier using LES model respect to RANS model. This behavior (effect of turbulence model on temperature and pressure) were observed for other initial gas temperatures in current work and have not reported herein.

As shown in Figure 3.19, RANS model is computationally less expensive respect to LES due to lower number of meshes. In the other word, RANS turbulence model sub-grid needs less number of cells respect to LES turbulence model. The comparison between predicted temperature profiles using RANS and LES models are shown in Figure 3.20. As it is well understood, RANS model is more diffusive than LES model; therefore, the temperature profile using RANS is more diffusive in radial direction as shown in Figure 3.20.

The spray and vapor penetrations using SAGE model and two turbulence models are shown in Figure 3.21. The liquid penetrations using both models are very similar but the LES turbulence model predict more fluctuations respect the RANS model. The n-dodecane vapor penetrates into combustion chamber more using LES model than RANS model. It confirms the previous conclusion that the RANS model is more diffusive in radial direction than axial direction.

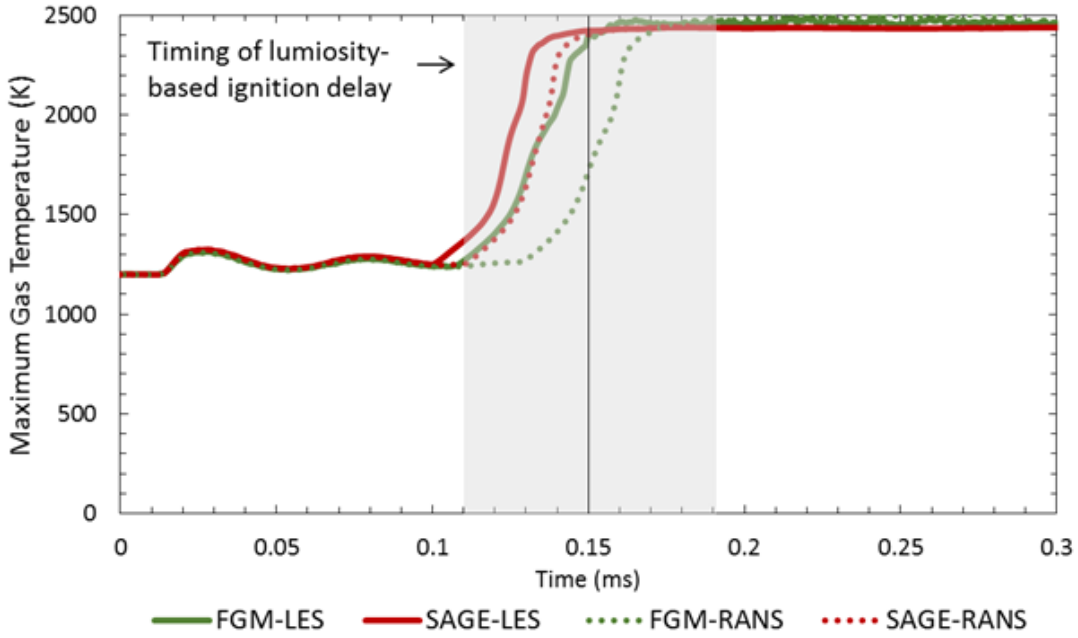

Figure 3.17 Maximum gas temperature at surrounding initial gas temperature of 1200 K and pressure of 79.4 bar

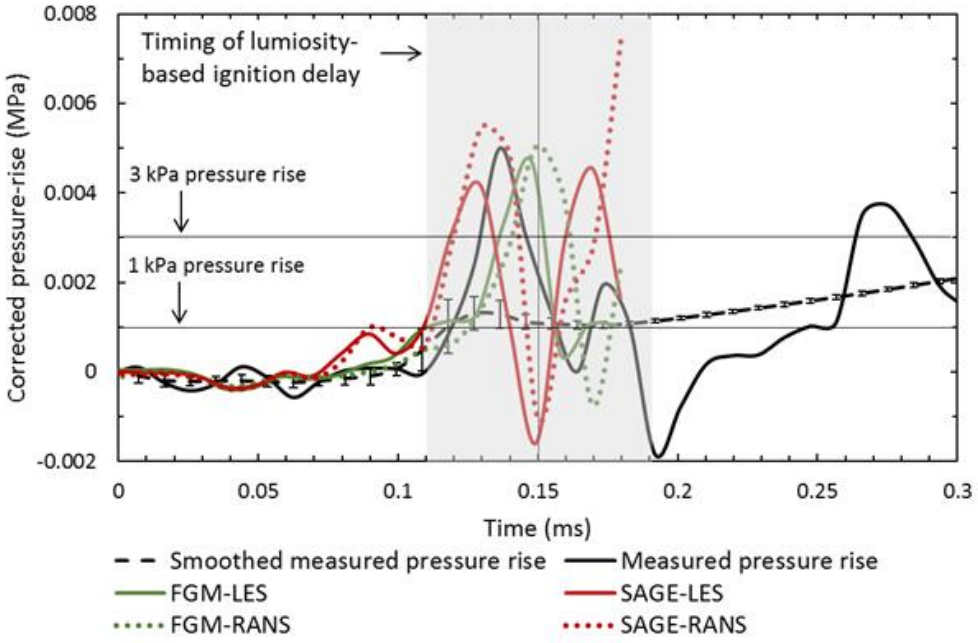

Figure 3.18 Corrected pressure-rise and measured data at surrounding initial gas temperature of 1200 K and pressure of 79.4 bar using two combustion and turbulence models

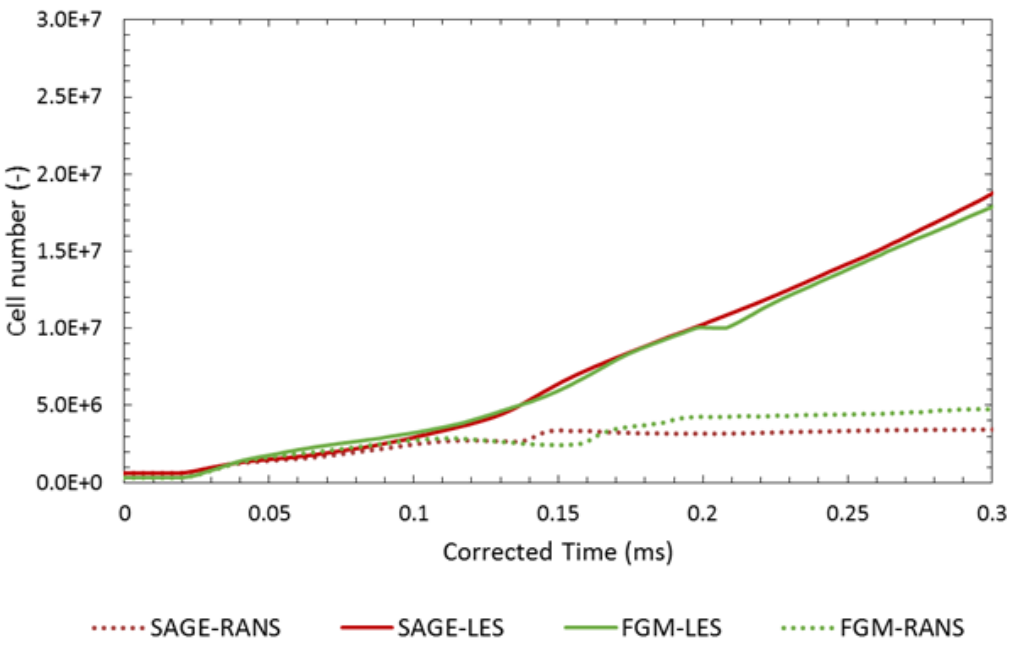

Figure 3.19 Total cell numbers at surrounding initial gas temperature of 1200 K and pressure of 79.4 bar

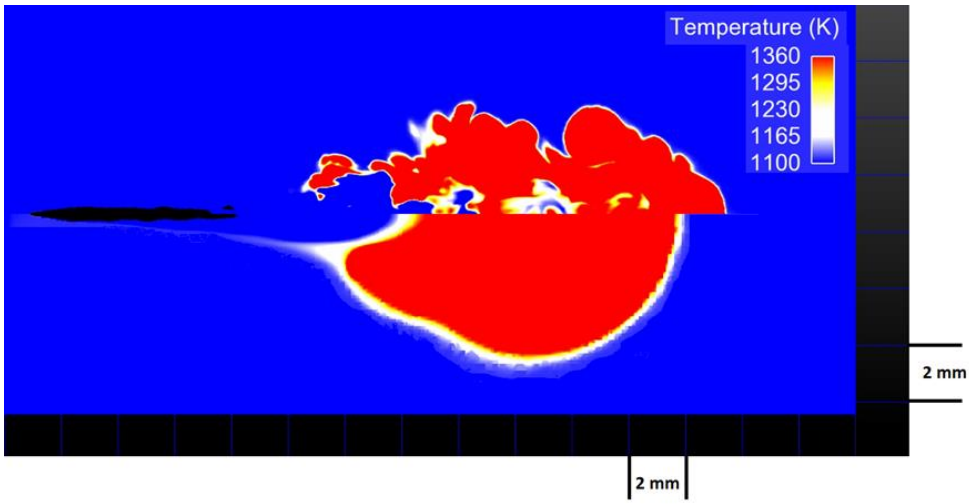

Figure 3.20 Temperature profile at initial gas temperature 1200 K using SAGE and two turbulence models, LES (upper image) and RANS (lower image) at 0.3 ms after start of injection

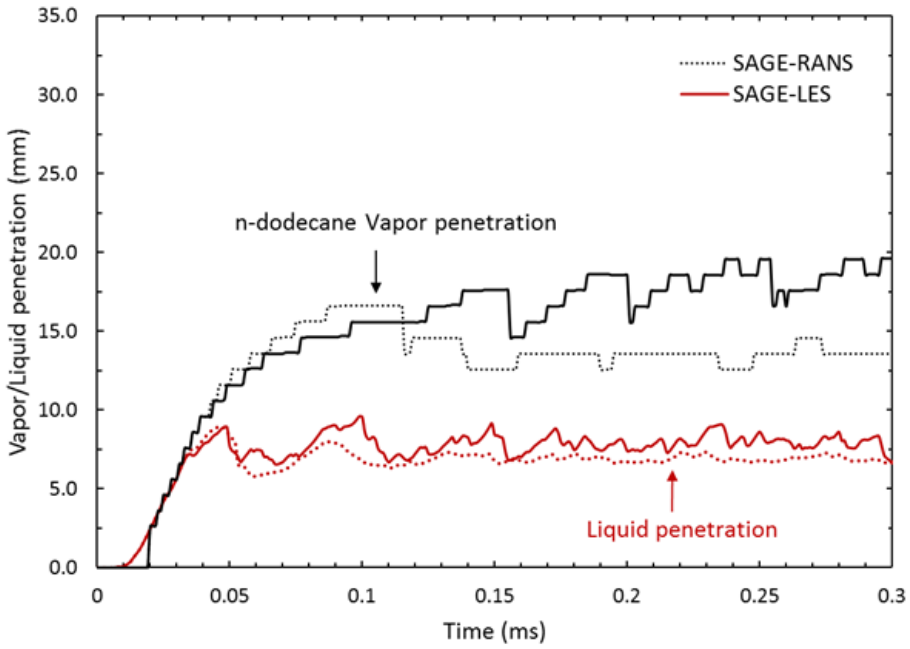

Figure 3.21 Liquid and vapor penetrations of turbulent spray combustion of n-dodecane at 1200 K using SAGE model and two turbulence models

3.5 Lift-Off Length

Lift-Off length (LOL) at various initial gas temperature is shown in Figures 3.22 to 3.25. The flame lift-off length is over predicted respect to measured data using RANS and SAGE models at all the studied initial gas temperatures. Flame lift-off length were predicted well using LES model and both combustion models for most of the studied initial gas temperatures, except at initial gas temperature of 900 K by using FGM. The steady state flame lift-off length at various temperatures are shown in Figure 3.26. Generally, the flame lift-off length decreases by increasing the initial gas temperature and the trend was well predicted by models.

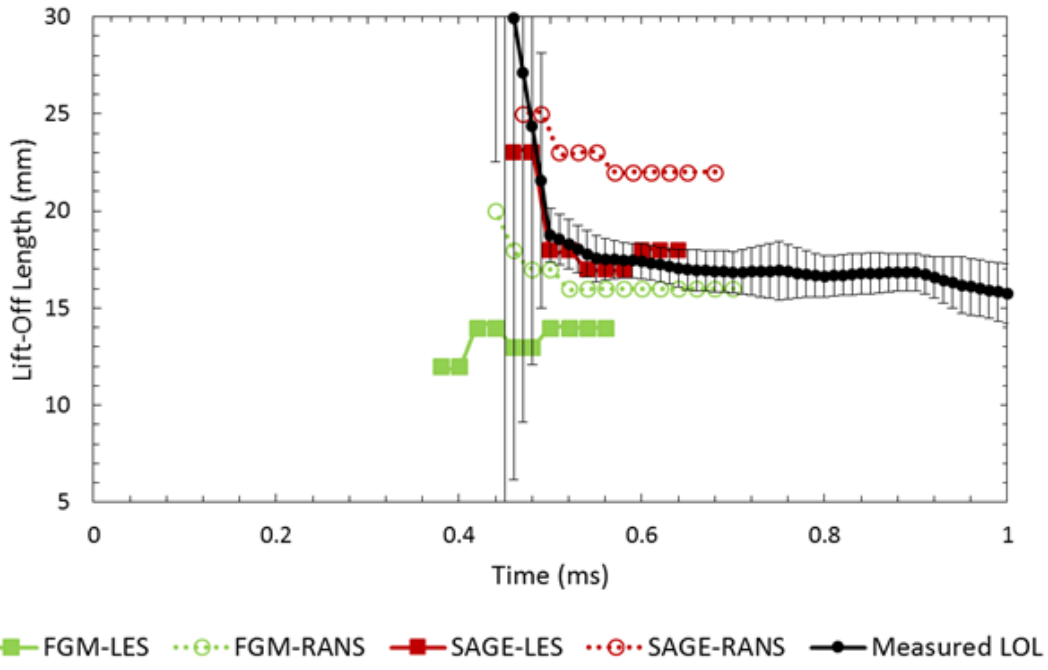

Figure 3.22 Flame lift-off length at initial gas temperature of 900 K using two combustion and turbulence models. The temperature thresholds of 2200 K were utilized for determining the lift-off length

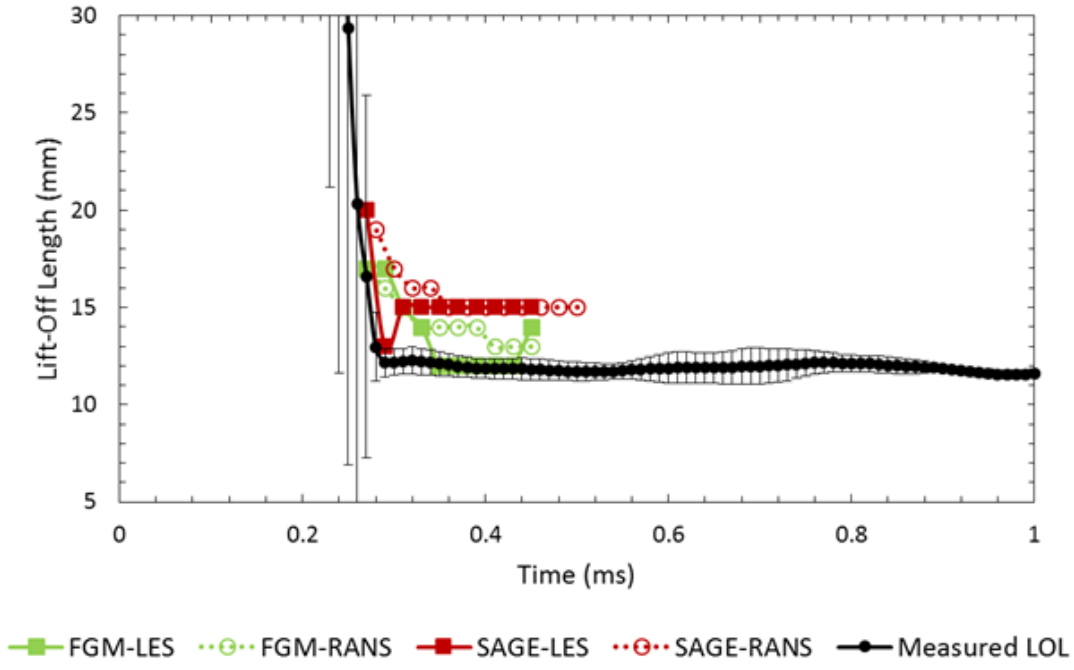

Figure 3.23 Flame lift-off length at initial gas temperature of 1000 K using two combustion and turbulence models. The temperature thresholds of 2300 K were utilized for determining the lift-off length

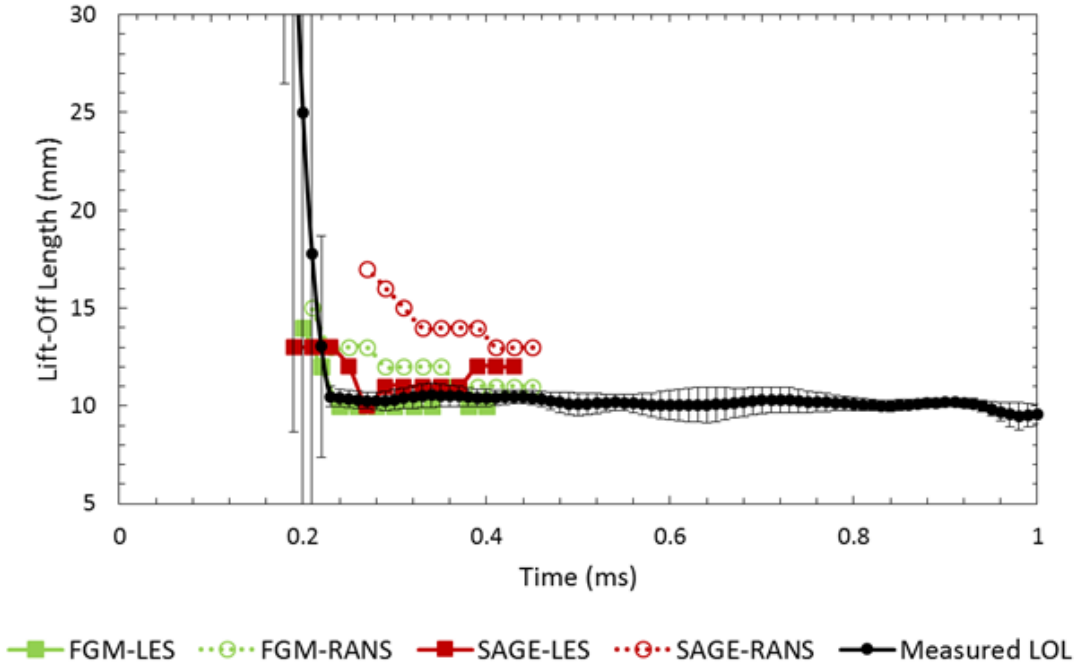

Figure 3.24 Flame lift-off length at initial gas temperature of 1100 K using two combustion and turbulence models. The temperature thresholds of 2350 K were utilized for determining the lift-off length

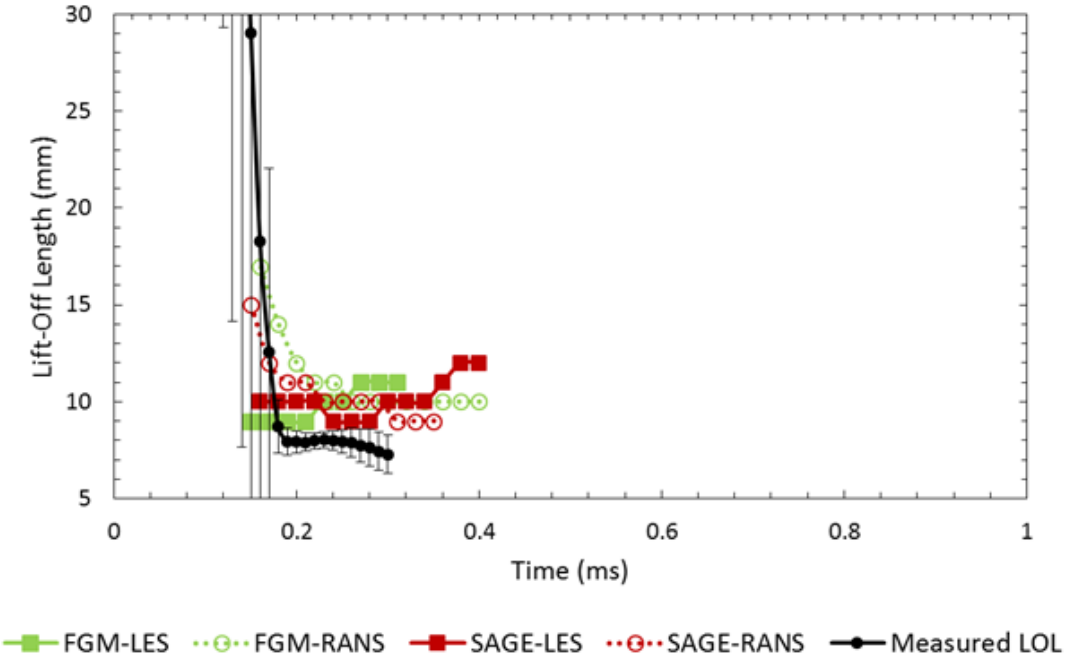

Figure 3.25 Flame lift-off length at initial gas temperature of 1200 K using two combustion and turbulence models. The temperature thresholds of 2450 K were utilized for determining the lift-off length

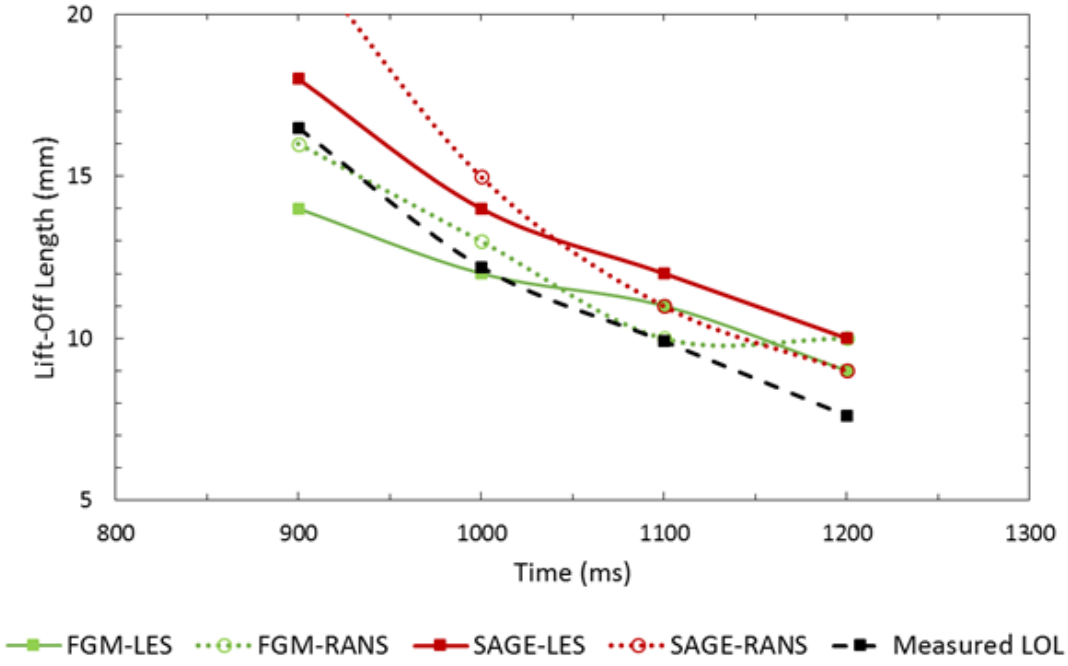

Figure 3.26 Flame lift-off length at various gas initial temperatures using two combustion and turbulence models

CHAPTER 4

4 CONCLUSIONS AND RECOMMENDATIONS

4.1 Conclusions

The turbulent spray combustion of n-dodecane at initial temperatures of 900 K, 1000 K, 1100 K, and 1200 K and gas density of 22.8 kg/m^3 was modeled using two combustion chemistry solvers -- direct integration chemistry solver (SAGE) and tabulated chemical kinetics solver Flamelet Generated Manifold (FGM) -- in a constant volume chamber (combustion vessel). Firstly, the effect of mesh size on pressure-rise due to combustion was modeled at 1200 K using tabulated chemistry and studied. Secondly, the performance of both the solvers was compared. Thereafter, two turbulence models, RANS and LES, were compared and finally flame lift-off length was compared using different combustion and turbulence models. In all cases, very fine mesh size of 31.25 microns was used around the spray to better capture the small eddies, and the embedding mesh and adaptive mesh refinement along with the skeletal n-dodecane chemical kinetics mechanism were also utilized to model turbulent spray combustion at the Spray A condition of ECN. The pressure rise, maximum gas temperatures, spray and vapor penetrations, and flame lift-off length were studied and compared with the experimental data. The following conclusions can be made by the current study:

1. Spray modeled pressure-rise is independent of mesh size if cylindrical shape embedded mesh with length of liquid penetration is utilized.

2. The measured spray to spray pressure-rise variations (fluctuations) can be modeled using various mesh sizes in the domain and embedded cylindrical shape with fixed mesh size around the spray.

3. Pressure-rise due to the combustion were well modeled in comparison with experimental data using both combustion models.

4. Both combustion models (SAGE and FGM) predicted the same behavior for pressure and temperature rises at high temperature such as 1100 K and 1200 K of initial gas temperature i.e. that the two models had similar sub-grid velocity and temperature conditions.

5. LES turbulence model sub-grid need more number of cells thus making it is computationally expensive.

6. The vapor penetration using RANS was under-predicted respect to LES since RANS model is more diffusive in radial direction respect to LES turbulence model.

7. Simulations using RANS-SAGE as compared to LES over-predicts the lift-off length.

8. Steady state flame lift-off lengths decreases by increasing the initial gas temperature was predicted well by both combustion and turbulence models.

4.2 Future Recommendations

1. Investigate the physics behind the early prediction of temperature rise by FGM at lower temperatures of 900 K and 1000 K.

2. Study the species histories using different chemistry solver and turbulence models.

3. Examine the numerical reason behind the over prediction of the flame lift-off length respect to measured data using RANS and SAGE models.

REFERENCES

[1] Heywood J.B., Internal Combustion Engine Fundamentals, 748-750 pages, McGraw-Hill, 1988.

[2] Bravo L., and Kweon C.B., "A Review on Liquid Spray Models for Diesel Engine Computational Analysis", Army Research Laboratory Technical Report Series, ARL-TR-6932, 2014.

[3] Senecal P. K., Pomraning E., Richards K., and Som S., "An Investigation of Grid Convergence for Spray Simulations using an LES Turbulence Model", SAE 2013-01-1083,2013.

[4] Samimi Abianeh O., "Study of Turbulent Spray Combustion of n-Dodecane Fuel", Proceedings of the ASME 2015 Internal Combustion Engine Division Fall Technical Conference, ICEF2015-1018, 2015.

[5] Goyal A., Samimi Abianeh O., and Bravo L., "Dependency of Turbulent Spray Combustion Modeling on Mesh Resolution Using Flamelet Generated Manifolds", 10th U. S. National Combustion Meeting Organized by the Eastern States Section of the Combustion Institute, College Park, MD, 2017.

[6] Samimi Abianeh O., Chen C. P., and Mahalingam S., "Numerical modeling of multi-component fuel spray evaporation process, International Journal of Heat and Mass Transfer", 69: 44-53, 2014.

[7] Senecal K., Pomraning E., Richards K.J., Briggs T.E., Choi C.Y., McDavid R.M., Patterson M. A., "Multi-dimensional modeling of direct-injection diesel spray liquid length and flame lift-off length using CFD and parallel detailed chemistry",

SAE World Congress & Exhibition, SAE 2003-01-1043, 2003.

[8] Lucchini T., D'Errico G., Onorati A., Frassoldati A., "Modeling Non-Premixed Combustion Using Tabulated Kinetics and Different Fame Structure Assumptions", SAE Int. J. Engines 10(2):593-607, 2017.

[9] Pickett L. M., Genzale C. L., Bruneaux G., Malbec L. M., Hermant L., Christiansen C., Schramm J., "Comparison of diesel spray combustion in different high-temperature, high-pressure facilities", SAE Int. J. Engines 3(2), 156–181, 2010.

[10] Pickett L. M., Manin J., Genzale C. L., Siebers D. L., Musculus M. P. B., Idicheria C. A., "Relationship between diesel fuel spray vapor penetration/dispersion and local fuel mixture fraction", SAE Int. J. Engines 4(1), 764–799, 2011.

[11] ECN: http://www.sandia.gov/ecn.

[12] Siebers D.L., "Liquid-Phase Fuel Penetration in Diesel Sprays", SAE Technical Papers, 1998.

[13] Weber J., Spiekermann P., Peters N., "Model Calibration for Spray Penetration and Mixture Formation in a High-Pressure Fuel Spray Using a Micro-Genetic Algorithm and Optical Data", SAE transactions 2005-01-2099, 2005.

[14] Kweon, C., "A Review of Heavy-Fueled Rotary Engine Combustion Technologies", ARL-TR- 5546; U.S. Army Research Laboratory: Aberdeen Proving Ground, MD, 2011.

[15] Payri, R., García-Oliver J. M., Bardi M., Manin J., "Fuel Temperature Influence on Diesel Sprays in Inert and Reacting Conditions", Applied Thermal Engineering 35, 185–195, 2012.

[16] Wang Y. J., Im K.-S., Fezzaa K., Lee W. K., Wang J., Micheli P., Laub C., "Quantitative X-Ray Phase-Contrast Imaging of Air-Assisted Water Sprays with High Weber Numbers", Applied Physics Letters October 89 (15)- 151913,2006.

[17] Coletti F., Benson M. J., Sagues A. L., Miller B. H., Fahrig R., Eaton J. K., "Three-Dimensional Mass Fraction Distribution of a Spray Measured by X-Ray Computed Tomography", ASME Journal of Engineering for Gas Turbines and Power, 2013.

[18] Senecal P., Richards K., Pomraning E., Yang T. A, "New Parallel Cut-Cell Cartesian CFD Code for Rapid Grid Generation Applied to in-Cylinder Diesel Engine Simulations", SAE 2007-01-0159, 2007.

[19] Amsden T. D., O'Rourke A. A., Butler P. J., "KIVA-II: A Computer Program for Chemically Reactive Flows with Sprays", LA-11560-MS, 1989.

[20] Vijayraghavan Iyengar S., Tsang C., Rutland C., "Validating Non-Reacting Spray Cases with KIVA-3V and OpenFoam", SAE technical paper 2013-01-1595, 2013.

[21] Bravo L., Kweon C.B., "Numerical Simulations of Evaporating Sprays in High Pressure and Temperature Operating Conditions Engine Combustion Network", ARL-TR-6938, May 2014.

[22] Samimi Abianeh O., Curtis N., and Sung C. J., "Determination of modeled luminosity-based and pressure-based ignition delay times of turbulent spray combustion", International Journal of Heat and Mass Transfer, 103: 1297-1312, 2016.

[23] Lebas R., Menard T., Beau P. A., Berlemont A., Demoulin F. X., "Numerical simulation of primary break-up and atomization: DNS and modelling study",

International Journal of Multiphase Flow 35(3), 247-260, 2009.

[24] Pomraning E., Richards K., and Senecal P., "Modeling Turbulent Combustion Using a RANS Model, Detailed Chemistry, and Adaptive Mesh Refinement", SAE Technical Paper 2014-01-1116, 2014.

[25] De Villiers E., Gosman A., Weller H., "Large Eddy simulation of primary diesel spray atomization", SAE World Congress & Exhibition, SAE 2004-01-0100, 2004.

[26] Som S., Senecal P. K., Pomraning E., "Comparison of RANS and LES Turbulence Models against Constant Volume Diesel Experiments", ILASS Americas, 24th Annual Conference on Liquid Atomization and Spray Systems, San Antonio, TX, 2012.

[27] Pope S. B., "Ten questions concerning the large-eddy simulation of turbulent flows", New Journal of Physics 6(35), 2004.

[28] Senecal P. K., Pomraning E., Richards K. J., Briggs T. E., Choi C. Y., McDavid R. M., Patterson M. A., "Multi-dimensional modeling of direct-injection diesel spray liquid length and flame lift-off length using CFD and parallel detailed chemistry", SAE World Congress & Exhibition, SAE 2003-01-1043, 2003.

[29] Van Oijen, and de Goey L, "Modelling of Premixed Laminar Flames using Flamelet-Generated Manifolds", Combust. Sci. Technol. 161(1): 113-137, 2000.

[30] Richards K. J., Senecal P. K., and Pomraning E., CONVERGE (Version 2.3) Manual, Convergent Science, Inc., Middleton, WI, 2016.

[31] Issa R. I., "Solution of Implicitly Discretized Fluid Flow Equations by Operator-

splitting," Journal of Computational Physics 6:240-65, 1986.

[32] Bravo L., Kurman M., Kweon C.B., Wijeyakulasuriya S., and Senecal P., "Lagrangian Modeling of Evaporating Sprays at Diesel Engine Conditions: Effects of Multi-Hole Injector Nozzles with JP-8 Surrogates", Proceeding of the 26th Annual Conference on Liquid Atomization and Spray Systems, 2014.

[33] Richards K. J., Senecal P. K., and Pomraning E., CONVERGE (Version 1.4.1) Manual, Convergent Science, Inc., Middleton, WI, 2012.

[34] Meijer M., Somers B., Johnson J., Naber J., Lee S., Malber L.M., Bruneaux G., Pickett L.M., Bardi M., Payri R., Bazyn T., "Engine Combustion Network (ECN): Characterization and Comparison of Boundary Conditions for Different Combustion Vessels", Atomization and Sprays 22 (9), 777–806, 2012.

[35] Pitz W., Westbrook C.K, Herbinet O., Silke E.J., "Progress in Chemical Kinetic Modeling for Surrogate Fuels", (LLNL-CONF-404514). In the 7th COMODIA International Conference on Modeling and Diagnostics for Advanced Engine Systems, 2008.

[36] Convergent Science, "CONVERGE Theory Manual". 6400 Enterprise Ln. Madison, WI 53719, 2015.

[37] Stiesch, G., "Modeling Engine Spray and Combustion Processes", Springer, 2003.

[38] Lin S. P., Reitz R. D., "Drop and Spray Formation from a Liquid Jet", Annual Review of Fluid Mechanics January, 30 (1), 85–105, 1998.

[39] Reitz R., Diwakar R., "Effect of Drop Breakup on Fuel Sprays", SAE Technical Paper 860469, 1986.

[40] Reitz R., "Computer Modeling of Sprays", Spray Technology Short Course, Pittsburgh, PA, 1996.

[41] Reitz R., Diwakar R., "Structure of High-Pressure Fuel Sprays", SAE Int.J.Engines 870598, 1987.

[42] Schmidt D. P., Rutland C. J., "A New Droplet Collision Algorithm", Journal of Computational Physics, 164(1): 62-80, 2000.

[43] Post S. L. and Abraham J., "Modeling the Outcome of Drop-drop Collisions in Diesel Sprays", International Journal of Multiphase Flow, 28(6): 997- 1019, 2002.

[44] Smith J. M., Van Ness H. C., and Abbott M. M, "Introduction to Chemical Engineering Thermodynamics", McGraw-Hill, 2005.

[45] B. Andersson, R. Andersson, L. Hakansson, M. Mortensen, R. Sudiyo, B. van Wachem, L. Hellstr, "Computational Fluid Dynamics for Engineers", 2012.

[46] CONVERGE: Advanced_Training_SAE2017.

[47] Pomraning E., "Development of Large Eddy Simulation Turbulence Models", Ph.D. Thesis, University of Wisconsin-Madison, 2000.

[48] Pope S. B., "Turbulent Flows", Cambridge University Press, 2000.

[49] D'Errico G., Lucchini T., Hardy G., Tap F. et al., "Combustion Modeling in Heavy Duty Diesel Engines Using Detailed Chemistry and Turbulence-Chemistry Interaction", SAE Technical Paper 2015-01-0375, 2015.

[50] Ferry T., and Schapotschnikow P., "Efficient Combustion Modeling Based on Tabkin® CFD Look-up Tables: A Case Study of a Lifted Diesel Spray Flame",

SAE 2012-01-0152, 2012.

[51] Dacolt Combustion & CFD Tabkin User Guide 2.1.1.

[52] Senecal P., Pomraning E., Richards K., Briggs T., "Multi-Dimensional Modeling of Direct-Injection Diesel Spray Liquid Length and Flame Lift-off Length using CFD and Parallel Detailed Chemistry", SAE Technical Paper 2003-01-1043, 2003.

[53] Lillo P., Pickett L., Persson H., Andersson O., "Diesel Spray Ignition Detection and Spatial/Temporal Correction", SAE Int. J. Engines 5(3), 1330-1346, 2012.

[54] Pickett L., Siebers D., and Idicheria C., "Relationship between Ignition Processes and the Lift-Off Length of Diesel Fuel Jets", SAE Technical Paper 2005-01-3843, 2005.

[55] Jansons M., Brar A., Estefanous F., Florea R., "Experimental Investigation of Single and Two-Stage Ignition in a Diesel Engine", SAE Technical Paper 2008-01-1071, 2008.

[56] Higuma A., Suzuki T., Yoshida M., Oguri Y., "Improvement of Error in Piezoelectric Pressure Transducer", SAE Technical Paper 1999-01-0207, 1999.

[57] Randolph A., "Methods of Processing Cylinder-Pressure Transducer Signals to Maximize Data Accuracy", SAE Technical Paper 900170, 1990.

[58] Higgins B., Siebers D., and Aradi A., "Diesel-Spray Ignition and Premixed-Burn Behavior", SAE Technical Paper 2000-01-0940, 2000.

ABSTRACT

TURBULENT SPRAY COMBUSTION MODELING USING DIRECT INTEGRATION OF CHEMISTRY AND FLAMELET GENERATED MANIFOLDS

by

ASHRAYA GOYAL

April 2017

Advisor: Dr. Omid Samimi

Major: Mechanical Engineering

Degree: Master of Science

Turbulent spray combustion of n-dodecane was modeled at engine relevant conditions using various combustion models (Direct Integration of Chemistry and Flamelet Generated Manifolds) and turbulence models (Dynamic Structure Large Eddy Simulation and RNG Reynolds-Averaged Naiver-Stokes). A recently developed n-dodecane mechanism was utilized and the turbulent spray was simulated at various combustion chamber initial gas temperature and pressure conditions. Mesh with size of 31 microns was utilized to resolve small eddies around the spray. The pressure-based ignition delay, flame lift-off length, and spray and jet penetrations were studied and compared with experimental measurements. The Direct Integration of Chemistry and Flamelet Generated Manifolds using various turbulence models are in agreement with measured data.

AUTOBIOGRAPHICAL STATEMENT

I was born in Indore, India on April 22, 1993. My keen interest in exploring and learning about the world of automobiles drove me to select engineering as my career path. I completed my Bachelor's degree in automobile engineering from Medicaps Institute of Science Technology, India in June 2015. Internal combustion engine being the heart of the automobiles, I elected thermal fluids as my specialization while I joined Wayne State University, Detroit, Michigan in August 2015 to pursue of the Master's degree in mechanical engineering.

After being through one year of coursework of my master's degree program, Prof. Dr. Omid Samimi-Abianeh gave me the opportunity to work in his Combustion Physics Lab and as a Graduate Teaching Assistant for the course of Intermediate Fluid Mechanics. I was both excited and thrilled for my first experience with research work. My research work mainly included CFD modeling in a constant volume combustion chamber with sprays. I extensively used CONVEGRE CFD solver and ENSIGHT post processing software to study pressure based ignition delays, liquid and vapor penetrations, and lift-off lengths. I have always believed in being curious and so my stride for the pursuit of knowledge continues as I look up to work in a company to test my knowledge in industry.